HEALTH AND MEDICINE

PTH treatment before cyclic joint loading improves cartilage health and attenuates load-induced osteoarthritis development in mice

Adrien Y. Antoinette[1]†, Sophia N. Ziemian[1]†, Allison R. Brown[1], Erin B. Hudson[1], Carolyn Chlebek[1], Timothy M. Wright[2], Steven R. Goldring[2], Mary B. Goldring[2], Miguel Otero[2,3], Marjolein C.H. van der Meulen[1,2]*

Osteoarthritis (OA) treatment is limited by the lack of effective nonsurgical interventions to slow disease progression. Here, we examined the contributions of the subchondral bone properties to OA development. We used parathyroid hormone (PTH) to modulate bone mass before OA initiation and alendronate (ALN) to inhibit bone remodeling during OA progression. We examined the spatiotemporal progression of joint damage by combining histopathological and transcriptomic analyses across joint tissues. The additive effect of PTH pretreatment before OA initiation and ALN treatment during OA progression most effectively attenuated load-induced OA pathology. Individually, PTH directly improved cartilage health and slowed the development of cartilage damage, whereas ALN primarily attenuated subchondral bone changes associated with OA progression. Joint damage reflected early transcriptomic changes. With both treatments, the structural changes were associated with early modulation of immunoregulation and immunoresponse pathways that may contribute to disease mechanisms. Overall, our results demonstrate the potential of subchondral bone-modifying therapies to slow the progression of OA.

INTRODUCTION

Concomitant changes in articular cartilage and the underlying subchondral bone are key contributors to osteoarthritis (OA) pathogenesis (*1*). The close mechanical and biological relationship between cartilage and subchondral bone suggests that alterations in subchondral bone properties, including changes in bone mass, stiffness, and remodeling, influence the health of the overlaying cartilage (*2*) and that tissue cross-talk is an important factor in OA disease (*3*).

Changes in subchondral bone mass and stiffness can modify both the stresses experienced by articular cartilage and the susceptibility to develop OA disease (*4*). Clinical studies reported conflicting results relating bone mass and OA pathology, with several studies demonstrating a positive relationship between bone mass and OA disease (*5*, *6*) and other work indicating that low bone mass is associated with increased cartilage damage and accelerated progression toward OA (*7*). In numerous preclinical studies, low bone mass or loss of bone mass before OA initiation exacerbated load-induced OA development (*8*–*11*). However, these studies examined the role of bone mass by comparing mouse strains with different intrinsic bone mass (*8*) or altered estrogen signaling (*9*–*11*), both of which also may directly affect cartilage and other joint tissues, thereby affecting OA susceptibility.

OA development also is associated with abnormal and increased subchondral bone remodeling, which likely plays an important role in OA pathology (*12*, *13*). Following OA initiation, a decoupling of normal bone resorption and formation occurs following an established pattern (*12*, *13*). In early-stage OA, an initial increase in bone resorption driven by increased osteoclast activity causes loss of subchondral bone mass, which is then followed by an increase in bone formation driven by increased osteoblast activity that ultimately results in subchondral bone sclerosis as OA progresses (*14*, *15*). Inhibiting these changes in bone remodeling immediately after OA initiation can reduce cartilage damage and OA progression in preclinical models, suggesting that early changes in bone remodeling are important to OA development (*16*–*18*).

The contributions of predisease subchondral bone properties, bone remodeling following disease initiation, and their interactions in OA development remain unclear. Most previous studies investigating the relationship between subchondral bone and OA development focused on tissue-level structural changes (*17*, *18*). While informative, tissue-level analyses provides a limited view of complex molecular interactions and joint tissue cross-talk contributing to OA development. Identifying time-dependent molecular changes associated with tissue-level outcomes across joint tissues during OA development would provide unique insight into the role of subchondral bone in disease development and the contribution of multiscale tissue interactions to disease progression. Recent genomics analyses of mouse whole knee joints (*19*, *20*) and articular cartilage (*21*–*24*) provided insight into the disease mechanisms underlying the development of OA. However, these studies did not address how changes in bone properties affect other joint tissues and modify disease progression. Given the multifactorial nature of OA, studies that examine concomitant changes in bone and different joint tissues are needed to understand organ-specific alterations during OA progression.

In the present study, we modulated subchondral bone properties in mice using two Food and Drug Administration–approved treatments for osteoporosis to examine the roles of subchondral bone mass, stiffness, and remodeling in OA development, integrating histopathological and transcriptomics analyses of multiple joint tissues. Parathyroid hormone (PTH), an anabolic osteoporosis treatment that increases bone mass and stiffness (*25*, *26*), was used to increase subchondral bone mass in vivo before OA initiation. Subchondral bone remodeling was reduced during OA

[1]Cornell University, Ithaca, NY, USA. [2]Hospital for Special Surgery, New York, NY, USA. [3]Weill Cornell Medicine, New York, NY, USA.
*Corresponding author. Email: mcv3@cornell.edu
†These authors contributed equally to this work.

progression using alendronate (ALN), an anticatabolic osteoporosis treatment that inhibits the resorptive capacity of osteoclasts (*27*, *28*). We subjected mice to daily tibial loading, a well-established model to initiate OA-like pathology and study load magnitude– and time-dependent changes in different tissues, including cartilage, bone, and lymph node (*8*, *18*, *29*–*31*).

We hypothesized that, under conditions of repetitive loading, increasing subchondral bone mass before OA initiation via PTH pretreatment and reducing subchondral bone remodeling via ALN treatment will attenuate the progression of OA. Specifically, we expected PTH pretreatment and ALN treatment to slow the development of load-induced cartilage damage observed histologically and subchondral bone loss. Furthermore, we expected attenuation in tissue damage to be associated with early-stage transcriptomic changes in cartilage, bone, and lymph nodes.

RESULTS

PTH pretreatment improved cartilage health and increased bone mass

We first determined the effects that PTH pretreatment had on both bone and cartilage baseline properties. We examined pretreatment-only groups, in which mice were euthanized after 8 weeks of PTH or vehicle (VEH) pretreatment (Fig. 1A). Limbs were analyzed for tissue-level changes using histology, microcomputed tomography (microCT), immunohistochemistry (IHC), and nanoindentation. RNA isolated from cartilage, bone, and lymph nodes of PTH- or VEH-pretreated groups was used for RNA sequencing (RNA-seq) analyses.

PTH-pretreated mice had thicker tibial cartilage than VEH mice ($P = 0.023$; Fig. 1, B and C). Cartilage structure, assessed by the OARSI score, was improved with PTH pretreatment, which led to a more pristine cartilage surface with fewer fibrillations and increased proteoglycan content ($P < 0.001$; Fig. 1C). PTH pretreatment decreased matrix metalloproteinase–13 (MMP-13) immunostaining in cartilage ($P = 0.036$) but did not alter runx-related transcription factor 2 (RUNX2) levels (Fig. 1, B and D). Cartilage stiffness, measured by nanoindentation, also was increased with PTH pretreatment compared to VEH ($P = 0.008$; Fig. 1E). Subchondral plate thickness (Fig. 1F) and subchondral plate tissue mineral density (TMD), assessed by microCT, were not altered by PTH pretreatment. PTH pretreatment increased cancellous bone volume fraction in the epiphysis ($P = 0.007$; Fig. 1F) and slightly decreased epiphysis TMD ($P = 0.050$). Bone remodeling in cancellous bone was increased in the PTH pretreatment group, as indicated by increased tartrate-resistant acid phosphatase (TRAP) ($P = 0.029$) and procollagen I ($P = 0.043$; Fig. 1, G and H) immunostaining. PTH pretreatment also decreased the relative number of sclerostin-positive osteocytes ($P = 0.015$; Fig. 1H). Overall, PTH pretreatment improved cartilage health and increased cancellous subchondral bone mass.

In RNA-seq analyses of different joint tissues, tibial cartilage displayed the most pronounced gene expression changes in response to PTH (Fig. 1I). Cartilage had 717 differentially expressed genes [DEGs; false discovery rate (FDR) < 0.05, fold change > 2], with 547 genes with higher expression in the PTH-pretreated group and 170 genes with higher expression in the VEH-treated mice. Lymph nodes had a total of 55 DEGs, cancellous bone had 40 DEGs, and cortical bone had 2. The expression of major genes with known roles in cartilage health and chondrocyte hypertrophy was not different in VEH- and PTH-pretreated groups (Fig. 1, J and K). Within cancellous bone, comparison of PTH and VEH groups did not identify changes in genes associated with osteoblast, osteoclast, or osteocyte activity (Fig. 1, J and K). On the basis of biological pathway enrichment analysis, relative to VEH-treated mice, the top five biological processes activated by PTH pretreatment in cartilage included changes in gene pathways associated extracellular matrix organization and several pathways associated with morphogenesis (Fig. 1L). The top five biological pathways suppressed by PTH pretreatment included changes in gene pathways associated with immune processes, including natural killer cell degranulation and neutrophil degranulation (Fig. 1L). No differentially enriched pathways were found in cortical bone, cancellous bone, or lymph nodes after 8 weeks of pretreatment. Overall, our transcriptomic analysis demonstrated PTH alters the expression of genes associated with cartilage homeostasis.

PTH pretreatment attenuated load-induced cartilage damage

Next, we examined whether the development of load-induced OA was influenced by the baseline subchondral bone mass or by bone remodeling. We applied daily mechanical loading for 1, 2, or 6 weeks to mice pretreated for 8 weeks with VEH or PTH to modulate baseline subchondral bone mass, followed by VEH or ALN treatment to inhibit bone remodeling, concomitant with loading for the duration of the loading period (Fig. 2A). A linear mixed-effects model was used to statistically assess the effects of loading (contralateral control versus loaded), duration (1, 2, or 6 weeks), pretreatment (PTH versus VEH), treatment (ALN versus VEH), and their interactions on each cartilage and subchondral bone measure.

Consistent with our previous studies using this loading protocol, daily cyclic compressive loading induced cartilage damage at all load durations in all pretreatment and treatment groups ($P < 0.001$; Fig. 2B), with increasing cartilage damage scores with longer load durations ($P < 0.001$). PTH pretreatment attenuated load-induced cartilage damage ($P < 0.001$; Fig. 2, B and C) throughout the entire joint, whereas inhibition of bone remodeling with ALN did not alter load-induced cartilage damage as measured by OARSI score. Cartilage damage was most severe in the posterior portion of the tibial plateau, but the effect of PTH pretreatment and ALN treatment on load-induced cartilage damage was similar throughout the joint. Whole-joint mean cartilage thickness was not altered by loading, pretreatment, or treatment. Localized cartilage thickness in the posterior region of the joint decreased with loading in a load duration–dependent manner ($P < 0.001$; Fig. 2D). ALN treatment attenuated the load-induced decrease in cartilage thickness at 6 weeks. Overall, PTH pretreatment attenuated load-induced cartilage damage, and ALN treatment had a more limited effect on cartilage damage after loading.

PTH pretreatment was chondroprotective and modulated load-induced RUNX2 and MMP-13 levels

We examined changes in cartilage protein levels at 1 week after initiation of daily loading using IHC analyses to identify the interactions between loading, PTH pretreatment, and ALN treatment on cartilage degradation. Cartilage tissue area with positive MMP-13 immunostaining, a collagenase with critical roles in type II collagen degradation (*32*), was decreased by both PTH pretreatment ($P = 0.013$) and ALN treatment ($P = 0.002$; Fig. 3, A and B). Load-induced changes in MMP-13 immunostaining depended on pretreatment ($P = 0.011$). MMP-13 levels increased with loading in VEH-pretreated groups but decreased in PTH-pretreatment groups. RUNX2 is a transcription factor with central

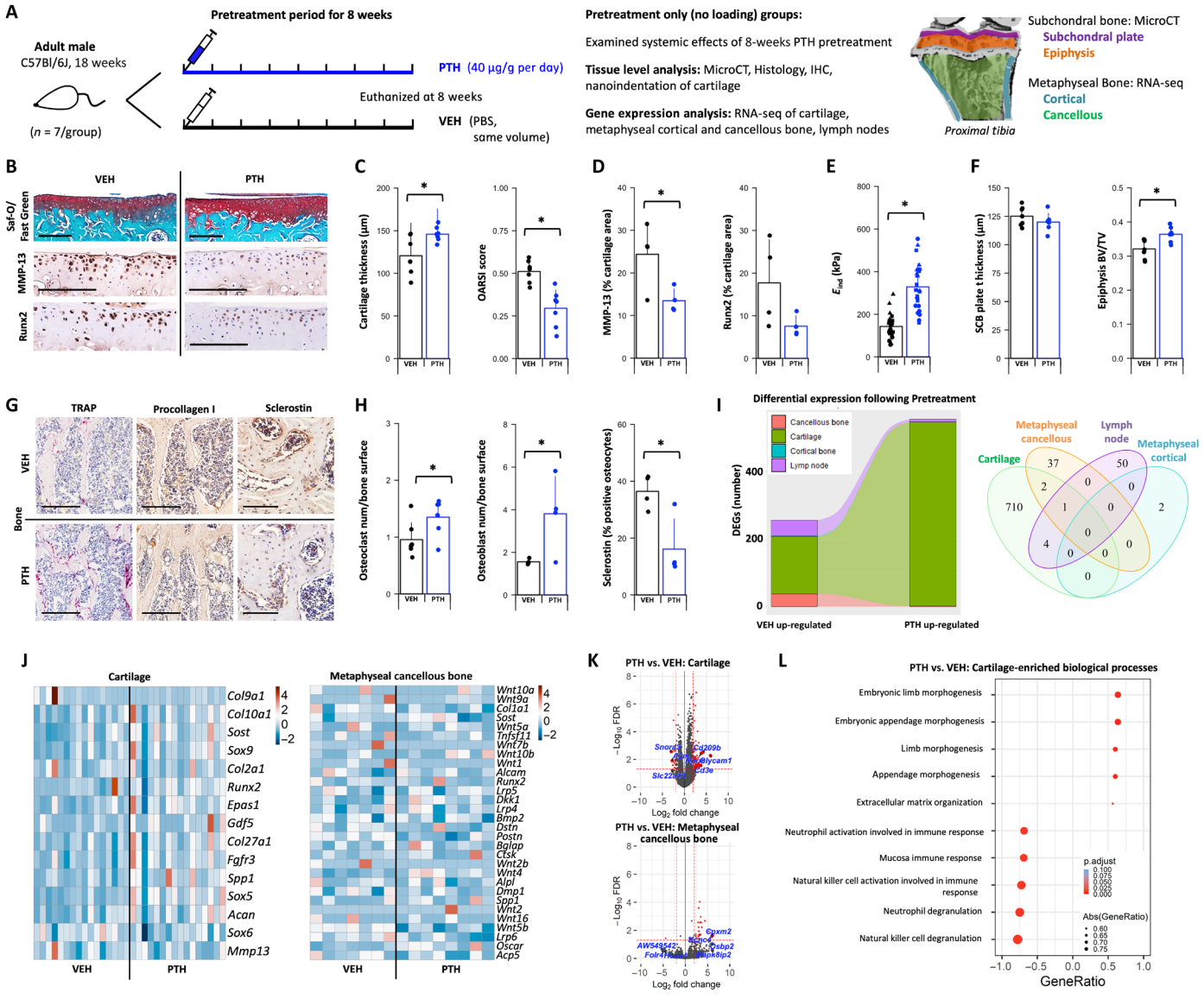

Fig. 1. PTH pretreatment alone altered cartilage and subchondral bone. (**A**) Mice underwent 8 weeks of PTH or VEH pretreatment to assess systemic effects. (**B**) Representative histology and IHC images of pretreated cartilage. Scale bar, 200 µm. In cartilage, PTH pretreatment (**C**) increased thickness and reduced histological score and (**D**) reduced MMP-13 expression but did not alter Runx2 expression. (**E**) PTH pretreatment increased cartilage stiffness. Each shape represents a single mouse ($n = 3$ per group, indentation speed = 1 µm/s). (**F**) PTH pretreatment did not alter subchondral plate thickness but increased bone volume fraction in the epiphysis. (**G**) Representative TRAP and IHC images of pretreated bone. (**H**) PTH pretreatment increased presence of osteoclasts and active osteoblasts and reduced sclerostin expression in osteocytes. (**I**) Alluvial plot and Venn diagram representation of the differentially expressed genes (DEGs) between PTH and VEH pretreatment in cartilage, cortical bone, cancellous bone, and lymph node [false discovery rate (FDR) < 0.05, fold change (FC) > 2]. (**J**) Heatmap representation of selected genes related to cartilage health and hypertrophy in cartilage and osteoblast, osteoclast, and osteocyte markers in cancellous bone. Data were *z*-score normalized. Both right and left limbs included. (**K**) Volcano plots representing DEGs in cartilage and cancellous bone. *FDR < 0.05 (**L**) Representation of the top five up-regulated and down-regulated Biological Processes enriched (adj.p < 0.05) for all significant genes in cartilage. *Bars indicate mean + SD. Individual data points ($n = 7$ per group) are overlaid. *$P < 0.05$ (*t* test).

roles in chondrocyte maturation, hypertrophy, endochondral ossification (*33*), and MMP-13 transcriptional activation (*34*) and has both anabolic and catabolic roles in OA cartilage (*35*). Tissue area with positive RUNX2 immunostaining was altered by loading ($P = 0.035$). RUNX2 levels increased with loading in VEH-pretreated groups but decreased with loading in PTH-pretreated groups ($P = 0.001$; Fig. 3, A and C). ALN treatment did not affect RUNX2 immunostaining in cartilage. Tissue area with positive type 1 PTH/PTHrP receptor (PTH1R) immunostaining, the primary PTH receptor on chondrocytes that decreases with OA progression (*36*), was not altered by PTH pretreatment ($P = 0.051$), ALN treatment or loading (fig. S1, A and B). Tissue area with positive sclerostin immunostaining, a Wnt inhibitor expressed by chondrocytes and implicated in OA progression (*37*), was decreased with PTH pretreatment ($P = 0.003$) and ALN treatment ($P = 0.003$; Fig. 3, A and D). PTH pretreatment also prevented the load-induced increases in sclerostin immunostaining in cartilage

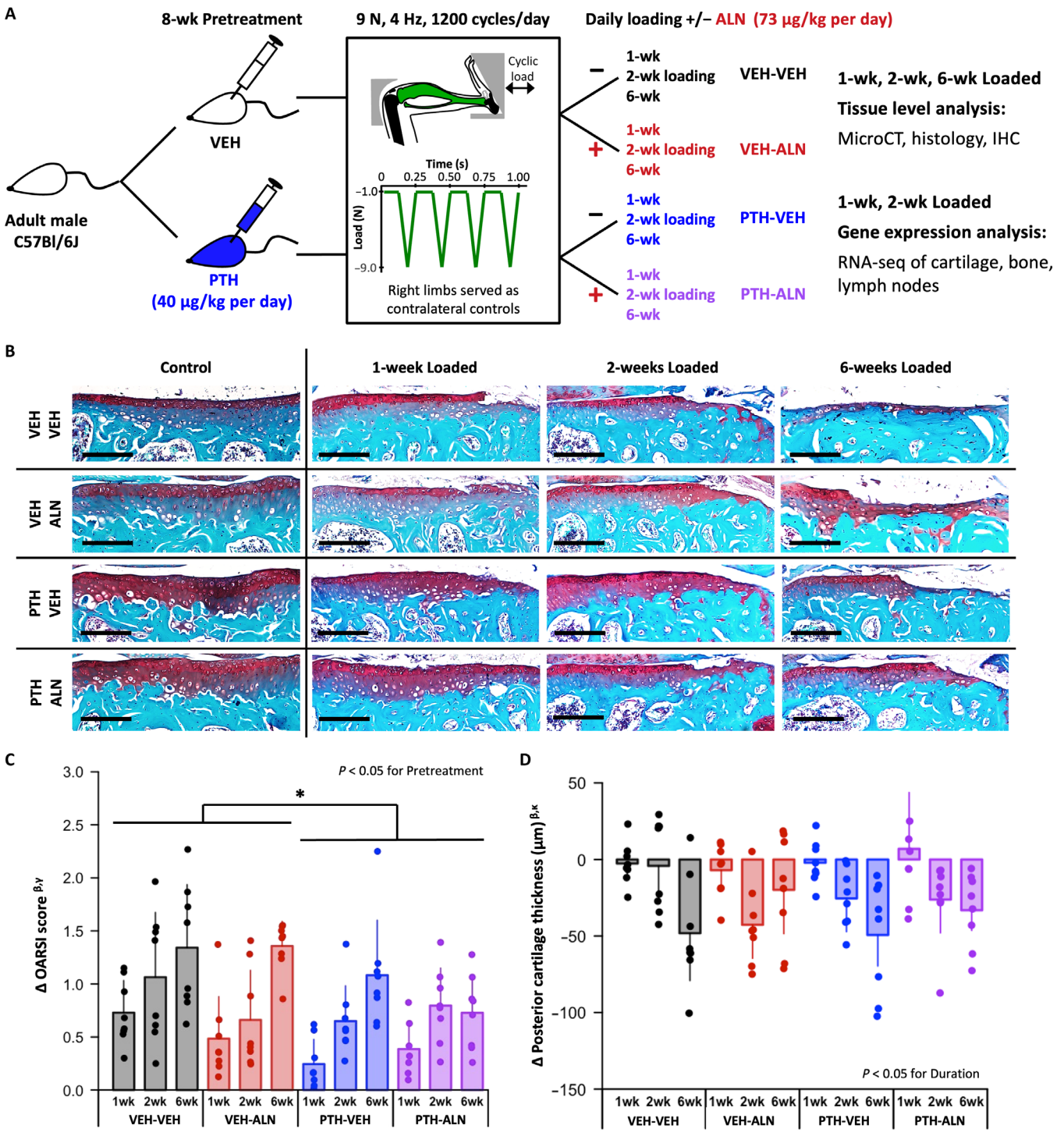

Fig. 2. PTH pretreatment attenuated load-induced cartilage damage. (**A**) Experimental design. (**B**) Representative histology images of cartilage damage following loading. Scale bar, 250 µm. (**C**) Cartilage damage increased with loading and the severity of load-induced cartilage damage was attenuated by PTH pretreatment. (**D**) Posterior cartilage thickness decreased with loading. Bars indicate mean + SD. Individual data points ($n = 8$ per group) are overlaid. Δ indicates difference between loaded and control limb measures within a single animal. $P < 0.05$ (linear mixed-effects model with Tukey's post hoc test) indicated on vertical axis for effects of $^{\beta}$Duration, $^{\gamma}$Pretreatment, $^{\kappa}$Duration × Treatment.

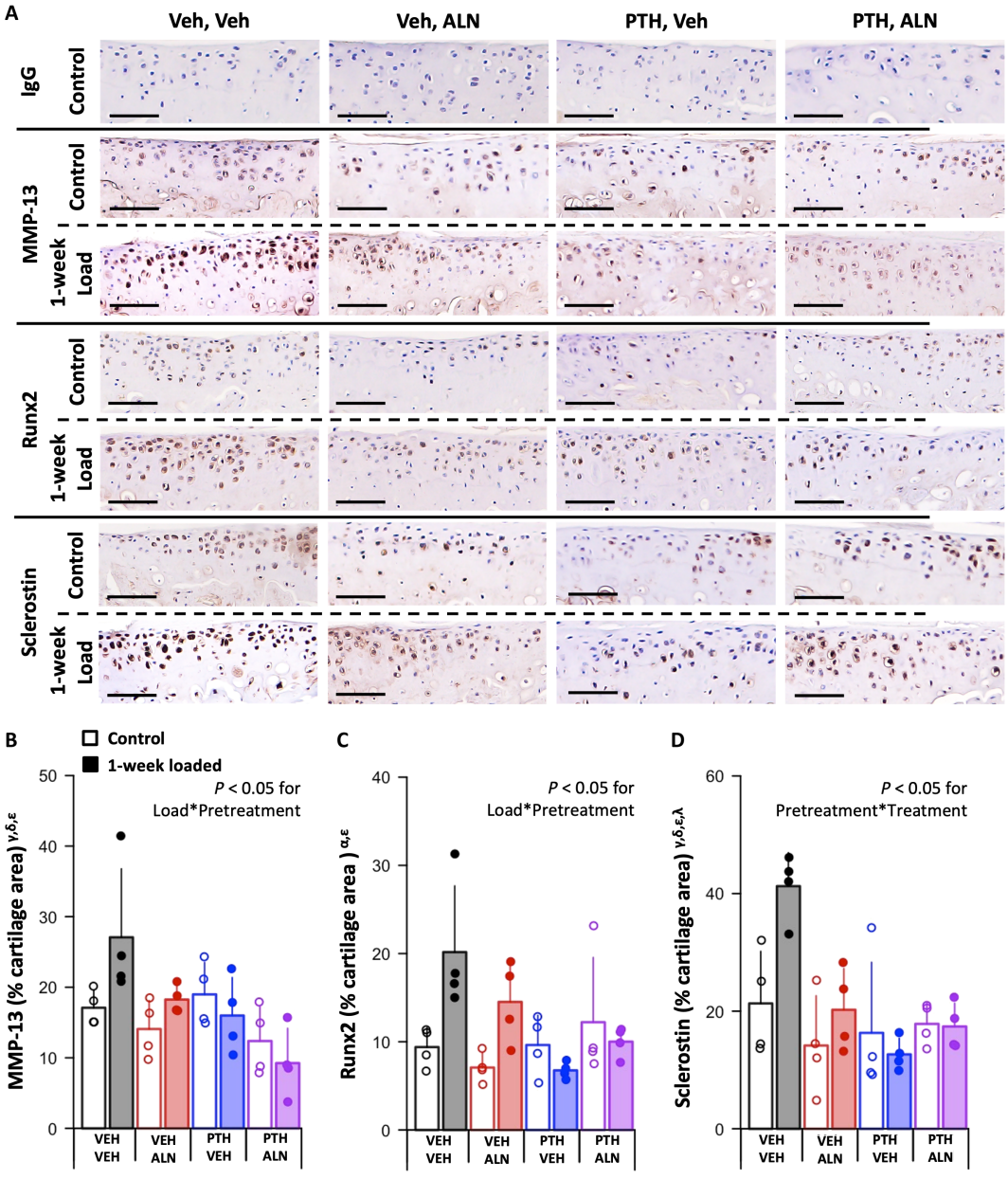

Fig. 3. PTH pretreatment and ALN treatment modulated load-induced protein expression changed in cartilage. (**A**) Representative IHC images of MMP-13, Runx2, and sclerostin expression in cartilage following 1 week of loading. Scale bar, 200 μm. (**B**) MMP-13 expression decreased with PTH pretreatment and ALN treatment. PTH pretreatment prevented the load-induced increase in MMP-13 expression. (**C**) PTH pretreatment prevented the load-induced increase in Runx2 expression. (**D**) Sclerostin expression decreased with PTH pretreatment and ALN treatment. PTH pretreatment prevented the load-induced increase in sclerostin expression. Bars indicate mean + SD. Individual data points ($n = 4$ per group) are overlaid. $P < 0.05$ (linear mixed-effects model with Tukey's post hoc test) indicated on vertical axis for effects of $^{\alpha}$Load, $^{\gamma}$Pretreatment, $^{\delta}$Treatment, $^{\varepsilon}$Load × Pretreatment, $^{\lambda}$Pretreatment × Treatment.

($P = 0.022$). Overall, PTH pretreatment attenuated load-induced increases in cartilage degrading enzymes and chondrocyte hypertrophy.

RNA-seq confirmed that articular cartilage is mechanosensitive and uncovered transcriptional responses to PTH and ALN

To further define cartilage responses, we performed RNA-seq analyses in RNA isolated from articular cartilage following 1 and 2 weeks of loading, from mice without and with pretreatment with PTH and treatment with ALN. First, we evaluated cartilage gene expression changes associated with load-induced OA-like pathology in the VEH-treated group, comparing load and control limbs (VEH-VEH comparison). We found a time-dependent increase in cartilage DEGs in response to loading, with 213 DEGs after 1 week of loading and 388 DEGs after 2 weeks of loading, with 150 overlapping DEGs (Fig. 4A). The expression of genes related to both

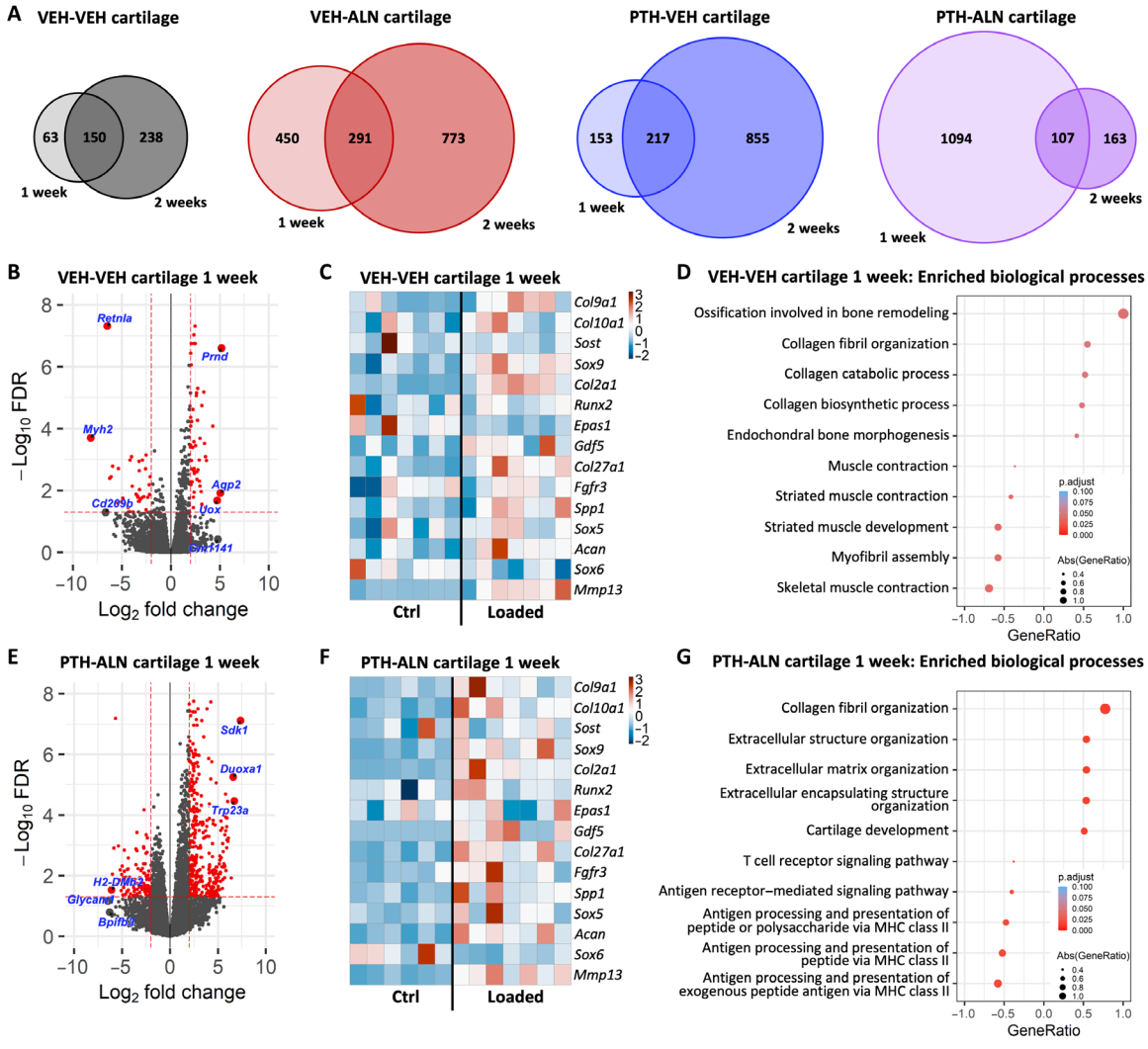

Fig. 4. Loading, pretreatment, and treatment induced transcriptomic changes in cartilage. (**A**) Venn diagram representation of the DEGs between 1 and 2 weeks of loading in cartilage for each treatment group (logFC > 1.5, FDR < 0.05). (**B**) Volcano plot representing DEGs for loaded relative to control limb VEH-VEH cartilage at 1 week (FDR < 0.05). (**C**) Heatmap representation of selected specific cartilage health and hypertrophic related genes for VEH-VEH cartilage. Data were *z*-score normalized. (**D**) Representation of the top five up-regulated and down-regulated Biological Processes enriched (adj.p < 0.05) for all significant genes comparing loaded and control VEH-VEH cartilage. (**E**) Volcano plot representing DEGs for loaded relative to control samples in PTH-ALN cartilage at 1 week (FDR < 0.05). (**F**) Heatmap representation of selected specific cartilage health and hypertrophic related genes for PTH-ALN cartilage. Data were *z*-score normalized. (**G**) Representation of the top five up-regulated and down-regulated Biological Processes enriched (adj.p < 0.05) for all significant genes comparing PTH-ALN loaded and control cartilage.

cartilage catabolic and anabolic processes, including *Mmp13*, *Spp1*, *Col9a1*, *Col27a1*, and *Gdf5*, increased with loading after 1 week (Fig. 4, B and C), consistent with both catabolic and anabolic responses associated with OA (*38*). *Sox9* expression was down-regulated at 2 weeks after loading, potentially indicating the loss of phenotypic stability of chondrocytes and a shift toward hypertrophic-like conversion (*39*). Load-induced changes in gene expression were less obvious after 2 weeks of loading (fig. S2), suggesting that gene expression changes leading to cartilage damage happen early during load-induced OA progression.

Top enriched biological pathways after 1 week of loading included collagen catabolic processes, ossification involved in bone remodeling, and endochondral bone (Fig. 4D), consistent with the proposed reactivation of developmental processes and hypertrophy-like conversion of OA chondrocytes (*40*). At 2 weeks of loading, enrichment was found in pathways associated with extracellular matrix organization, endochondral ossification processes, and myofibril organization (fig. S2), consistent with the proposed loss of phenotypic regulation of OA chondrocytes (*40*), including fibroblast-like changes in late disease stages (*41*). Overall, the early transcriptomic responses of cartilage to loading correlated to the structural damage observed at later time points.

Next, we examined changes in gene expression in cartilage in response to loading with PTH pretreatment and ALN treatment. We found an overall increase in DEGs in all treatment groups and time points relative to the VEH-VEH treated group, except for decreased DEGs in the PTH-ALN group at 2 weeks (Fig. 4A). In the VEH-ALN group, we identified a time-dependent increase in DEGs, with

1064 genes after 2 weeks relative to 741 genes after 1 week, with 291 overlapping DEGs. Similarly, the PTH-VEH group also displayed an increase in DEGs over time, with 1072 DEGs at 2 weeks versus 370 DEGs at 1 week and 217 overlapping DEGs. In contrast, the PTH-ALN treatment had more genes differentially expressed after 1 week of loading (1201 genes) relative to the 2-week time point (270 genes), with 107 of these genes shared between time points. Two hundred fifty-four of the DEGs present at 1 week in the PTH-ALN group were then present at 2 weeks in the VEH-VEH group. Together, these results suggest that the combined PTH-ALN treatment shifted the temporal responses of cartilage to loading.

Because the PTH-ALN cotreatment group displayed the most pronounced tissue-level changes across cartilage and bone, we performed additional analyses of the pretreatment and treatment effects in this group. With combined PTH-ALN treatment, the expression of genes traditionally used to define healthy articular chondrocytes and cartilage anabolism, including *Acan*, *Col2a1*, and *Sox9*, was increased in the loaded limb after 1 week (Fig. 4, E and F). We also identified a concomitant increase in the expression of genes related to cartilage catabolism and chondrocyte hypertrophy, including *Col10a1*, *Mmp13*, and *Spp1*. After 1 week of loading, extracellular matrix organization and cartilage development were among the top five up-regulated biological processes with loading (Fig. 4G). The five most down-regulated biological processes were all associated with antigen presentation via major histocompatibility complex class II and T cell receptor signaling.

Overall, these loading-based differences were less evident after 2 weeks of loading (fig. S2). Similar analyses were performed on the VEH-ALN and PTH-VEH groups (figs. S2 and S3). Together, our analyses suggest that the combination of PTH pretreatment and ALN treatment leads to more rapid and potent anabolic responses and decreased catabolic responses in articular chondrocytes in response to loading, which concur with the reduced structural damage in cartilage observed in this treatment group.

ALN treatment slowed osteophyte development

Osteophyte formation is a hallmark of OA disease (*42*). We used established histological methods to assess osteophyte formation, size, and maturity (*43*) to determine whether PTH pretreatment or ALN treatment altered ectopic bone formation resulting from load-induced OA. Consistent with the OA-like pathology previously reported in this mouse model (*8*, *29*), medial tibial osteophytes formed with loading in all groups (Fig. 5A), and osteophyte size and maturity increased with load duration ($P < 0.001$; Fig. 5, A to C). Osteophyte size decreased with both PTH pretreatment ($P = 0.035$) and ALN treatment ($P = 0.021$; Fig. 5B), whereas osteophyte maturity decreased with ALN treatment ($P < 0.001$; Fig. 5C) but was not altered by PTH pretreatment. In ALN-treated groups, osteophytes remained partially cartilaginous at 6 weeks after initiation of loading, whereas osteophytes were fully calcified at 6 weeks in VEH-treated groups. Overall, our findings confirm that ALN treatment slowed osteophyte development, as indicated by decreased osteophyte size and maturity following loading, whereas PTH pretreatment only reduced osteophyte size.

ALN treatment systemically increased subchondral bone mass

Next, we examined subchondral bone changes in the cortical subchondral plate and the epiphysis using microCT analysis to determine the effects of PTH pretreatment, ALN treatment, and loading. Consistent with previous results (*8*), subchondral cortical plate thickness decreased with mechanical loading ($P = 0.001$; Fig. 5D). ALN treatment increased subchondral plate thickness ($P = 0.009$; fig. S4) but did not alter the load-induced loss of subchondral plate thickness (Fig. 5D). PTH pretreatment did not alter subchondral plate thickness or the change in thickness with loading. Epiphysis bone volume/total volume (BV/TV) decreased with mechanical loading ($P < 0.001$; Fig. 5E). ALN treatment increased BV/TV ($P < 0.001$; fig. S4) and attenuated the load-induced decrease in BV/TV ($P < 0.001$; Fig. 5E). PTH pretreatment increased BV/TV ($P = 0.004$; fig. S4) but did not alter the response to mechanical loading. Overall, loading decreased subchondral bone mass and ALN treatment attenuated cancellous subchondral bone changes, whereas PTH pretreatment did not alter load-induced bone changes.

ALN treatment reduced bone remodeling

To understand the impact of loading, PTH pretreatment, and ALN treatment in bone cells, we performed immunostaining of markers for osteoclasts (TRAP), osteoblasts (procollagen I) and osteocytes (sclerostin). TRAP staining increased in cells in the epiphyseal bone with PTH pretreatment ($P = 0.003$), in agreement with our assessment of changes at baseline, and decreased with ALN treatment ($P < 0.001$; Fig. 5, F and G). Load-induced changes in $TRAP^+$ cells depended on PTH pretreatment ($P = 0.040$) and ALN treatment ($P < 0.001$): Tibial loading induced an increase in $TRAP^+$ immunostaining in the VEH-treated groups, but pretreatment with PTH or treatment with ALN prevented the load-induced changes. The presence of active osteoblasts, examined through procollagen I IHC, was decreased with ALN treatment ($P < 0.001$) but not altered by PTH pretreatment or loading (Fig. 5, F and H). The relative number of sclerostin positive osteocytes was decreased by both PTH pretreatment ($P < 0.001$) and ALN treatment ($P < 0.001$) but not altered by loading (fig. S5). Together, these findings suggest that ALN attenuated bone remodeling and that both PTH pretreatment and ALN treatment altered load-induced changes in osteoclasts presence, likely reducing load-induced bone resorption.

PTH pretreatment and ALN treatment attenuated transcriptional responses to loading in bone

To further evaluate the responses of bone to loading without or with PTH pretreatment and ALN treatments, we performed RNA-seq analyses of RNA isolated from cortical and cancellous metaphyseal bone at 1 and 2 weeks after initiation of loading. Analyses of the VEH-VEH group showed that the number of load-induced DEGs was similar at 1 and 2 weeks (280 versus 288; Fig. 6A), with 18 DEGs common to both time points. The five most suppressed biological processes in cortical bone after loading included positive regulation of T cell mediated immunity, neutrophil activation, and granulocyte activation (Fig. 6, B to D). Cancellous bone was less responsive to loading, with only 18 DEGs at 1 week and no DEGs at 2 weeks (Fig. 6G).

Next, we examined responses to the PTH pretreatment and ALN treatment relative to the VEH-VEH group. Overall, fewer load-induced DEGs were present in the cortical bone of ALN and PTH groups relative to the VEH-VEH group. The VEH-ALN group had two DEGs at 2 weeks after initiation of loading and none after 1 week (Fig. 6A). The PTH-VEH group had 92 DEGs at 1 week after loading and 17 DEGs at 2 weeks, with seven genes shared between time

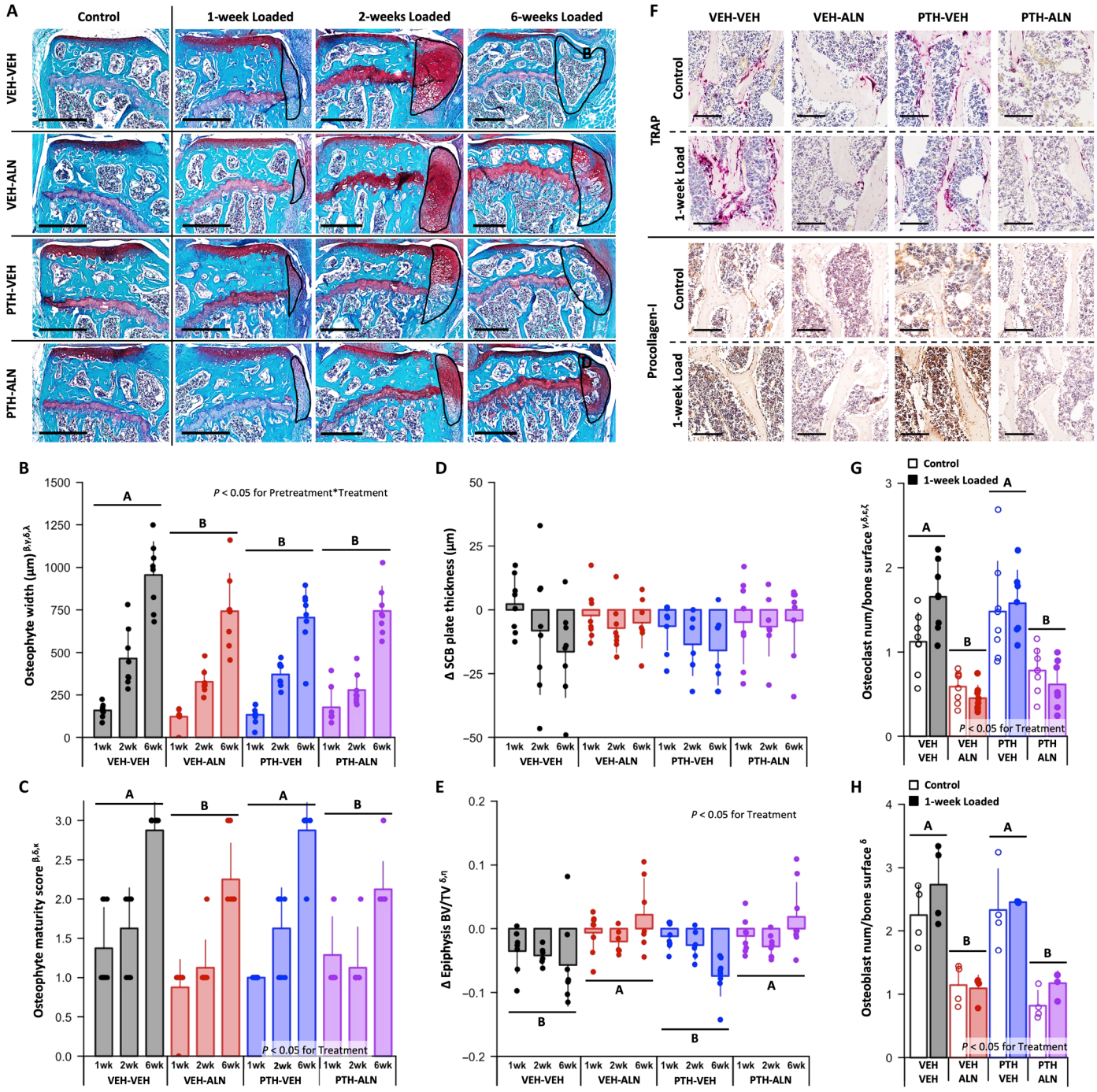

Fig. 5. ALN treatment attenuated bone changes. (**A**) Representative histology images of osteophyte formation following loading. Scale bar, 500 µm. (**B**) Both PTH pretreatment and ALN treatment decreased the width of osteophytes formed in loaded limbs. (**C**) ALN treatment slowed calcification of osteophytes at 2 and 6 weeks. (**D**) Neither PTH pretreatment or ALN treatment altered the load-induced decreased in subchondral plate thickness. (**E**) ALN treatment attenuated load-induced decreased in epiphysis TMD. (**F**) Representative IHC images of TRAP (osteoclasts) and procollagen I (active osteoblasts) in bone following 1 week of loading. Scale bar for TRAP and procollagen I, 200 µm. (**G**) ALN treatment decreased presence of osteoclasts. (**H**) ALN treatment decreased presence of active osteoblasts. Bars indicate mean + SD. Individual data points ($n = 8$ per group) are overlaid. Δ indicates difference between loaded and control limb measures within a single animal. $P < 0.05$ (linear mixed-effects model with Tukey's post hoc test) indicated on vertical axis for effects of $^{\beta}$Duration, $^{\gamma}$Pretreatment, $^{\delta}$Treatment, $^{\kappa}$Duration × Treatment, $^{\lambda}$Pretreatment × Treatment, $^{\epsilon}$Load × Pretreatment.

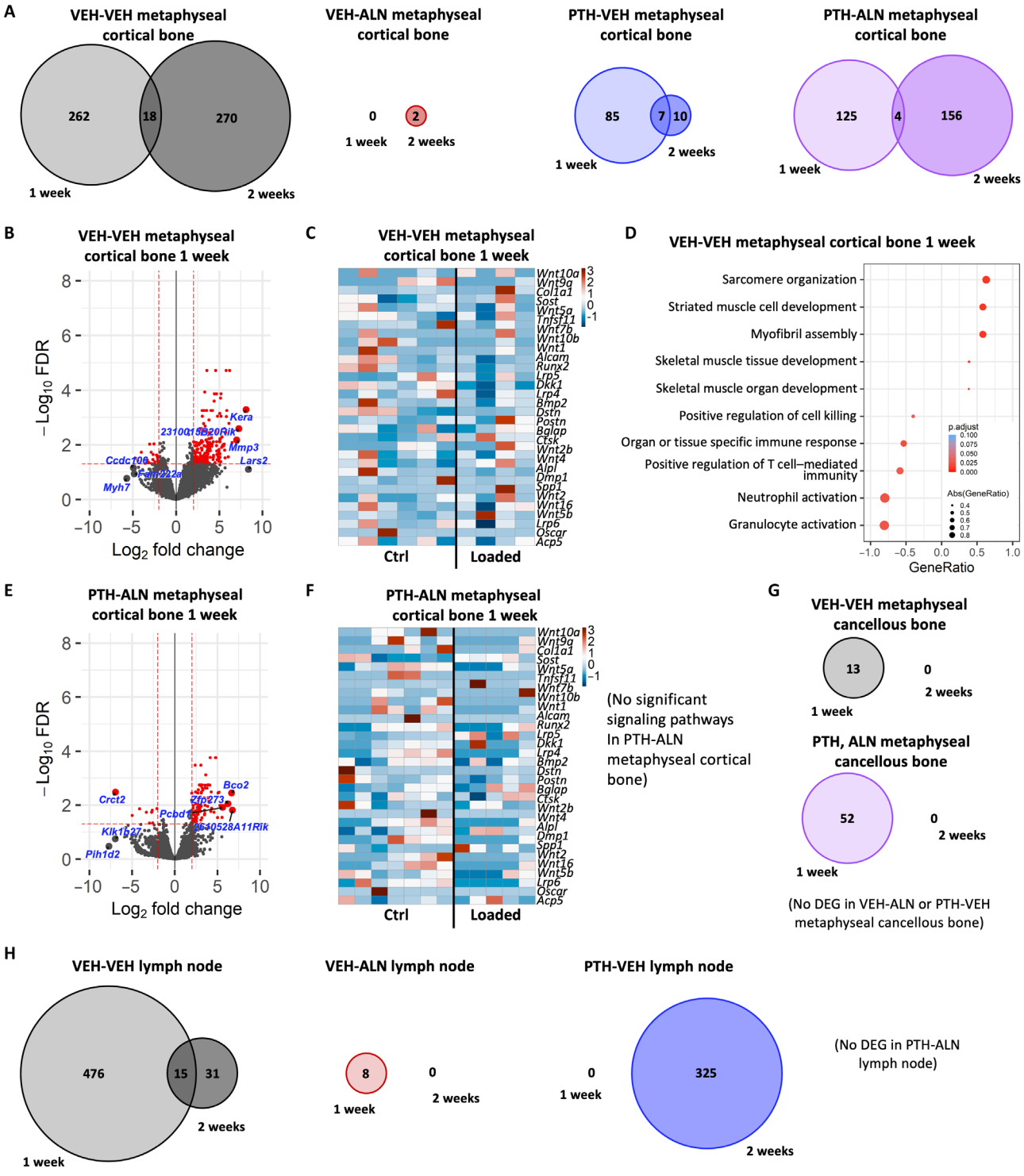

Fig. 6. Loading, pretreatment, and treatment induced transcriptomic changes in bone and lymph node. (**A**) Venn diagram representation of the DEGs between 1 and 2 weeks of loading in metaphyseal cortical bone for each treatment group (logFC > 1.5, FDR < 0.05). (**B**) Volcano plot representing DEGs for loaded relative to control limb VEH-VEH metaphyseal cortical bone at 1 week (FDR < 0.05). (**C**) Heatmap representation of selected specific osteoblast, osteoclast, and osteocyte marker genes in metaphyseal cortical bone. Data were *z*-score normalized. (**D**) Representation of the top five up-regulated and down-regulated Biological Processes enriched (adj.p < 0.05) for all significant genes comparing loaded and control VEH-VEH metaphyseal cortical bone. (**E**) Volcano plot representing DEGs for loaded relative to control limb PTH-ALN metaphyseal cortical bone at 1 week (FDR < 0.05). (**F**) Heatmap representation of selected specific osteoblast, osteoclast, and osteocyte marker genes in PTH-ALN metaphyseal cortical. Data were *z*-score normalized. (**G**) Venn diagram representation of the DEGs between 1 and 2 weeks of loading in metaphyseal cancellous bone for each treatment group (logFC > 1.5, FDR < 0.05). (**H**) Venn diagram representation of the DEGs between 1 and 2 weeks of loading in lymph nodes for each treatment group (FC > 2, FDR < 0.05).

points. In contrast, the PTH-ALN group displayed more DEGs after 2 weeks of loading (160 genes) compared to 1 week (132 genes), with only four overlapping DEGS. Similar to the findings in the VEH-VEH group, the cancellous bone was less responsive, and we only identified 52 load-induced DEGs at 1 week in the PTH-ALN group (Fig. 6G).

Because the tissue-level analyses showed more prominent changes in the PTH-ALN group, we performed additional analyses in this dataset. In cortical bone, genes related to Wnt signaling were downregulated after 1 week of loading in the PTH-ALN group (Fig. 6, E and F). Expression of genes related to osteoblasts and osteoclasts in cancellous bone had no clear trend with loading in the PTH-ALN group. No biological pathway was enriched in the cortical or cancellous bone in the PTH-ALN treatment group at 1 week. Similar results were found in the VEH-ALN and PTH-VEH groups (figs. S6 and S7).

Loading induced transcriptomic changes in lymph nodes that attenuated over time

To examine immune responses, we performed RNA-seq analyses in the inguinal lymph nodes after 1 and 2 weeks of loading. Comparison of the VEH-VEH groups showed rapid responses to loading, with 491 DEGs at 1 week that quickly attenuated to 46 DEGs at 2 weeks and 15 DEGs shared between time points (Fig. 6H). In the VEH-ALN, a small number of DEGs were present at 1 week after initiation of loading (eight genes) and none present after 2 weeks. In contrast, DEGs were only present after 2 weeks of loading in the PTH-VEH group (325 genes). No DEGs were present in the PTH-ALN group. Enriched biological pathways were present in the VEH-VEH and VEH-ALN groups at 1 week but not in the PTH-VEH or PTH-ALN groups (fig. S8).

The estimated fractions of B cells, $CD4^+$ T cells, and $CD8^+$ T cells, as calculated by CIBERSORT using gene expression profiles (*44*), were altered by ALN treatment (fig. S9). The fraction of $CD8^+$ T cells increased with ALN treatment following 1 week of loading ($P = 0.033$). Following 2 weeks of loading, the fraction of B cells decreased with ALN treatment ($P = 0.018$), and the fraction of $CD4^+$ T cell increased with ALN treatment ($P = 0.009$). Overall, ALN treatment during loading modulated the presence of immune cells in the lymph node, but PTH had little effect.

DISCUSSION

In the present study, we examined the role of subchondral bone properties in OA development and progression by determining the effect of bone-modulating therapies in attenuating damage severity. We also sought to understand the spatiotemporal progression of joint damage in OA disease by combining histopathologic and transcriptomic analyses. Our findings partially support our hypothesis as both bone-modulating therapies approved to treat osteoporosis slowed aspects of OA progression. The additive effect of PTH pretreatment before OA initiation combined with ALN treatment during damage progression most effectively attenuated load-induced pathology across the whole joint. PTH pretreatment slowed the development of cartilage damage and may have shifted chondrocyte phenotype, whereas ALN treatment attenuated osteophyte formation and subchondral bone changes associated with OA progression. We cannot distinguish whether decreased OA development with PTH pretreatment specifically resulted from increased predisease subchondral bone mass or, more likely, from a combination of increased bone mass and direct effects on predisease cartilage properties.

Consistent with our previous reports (*8*, *18*, *29*, *30*), daily cyclic tibial loading induced joint damage in a duration-dependent manner. Using PTH pretreatment before loading and ALN treatment concurrent with loading altered the progression of OA-like pathology. PTH-pretreated mice had increased cancellous bone mass, fewer cartilage surface fibrillations, increased proteoglycan staining, and decreased MMP-13 immunostaining before loading. With loading, PTH pretreatment decreased the severity of load-induced cartilage damage and prevented the load-induced increase of matrix-degrading enzymes (MMP-13) and markers of chondrocyte hypertrophy (RUNX2) in cartilage. On the basis of these results, the PTH-induced prevention of cartilage damage was mediated, at least in part, by reduced RUNX2 and MMP-13 levels, consistent with reports in MMP-13 and RUNX2 knockout mice (*43*, *45*). Furthermore, our findings suggest that PTH had direct effects in cartilage, similar to prior work examining PTH treatment following osteochondral defects or collagenase-induced cartilage damage (*46*, *47*). PTH pretreatment also decreased osteophyte growth but did not slow osteophyte maturity or alter the subchondral bone response to loading. PTH pretreatment increased bone remodeling and inhibited sclerostin production by osteocytes, a potential mechanism through which PTH has an anabolic effect on bone (*48*).

In contrast, ALN treatment concurrent with daily loading attenuated OA-related changes in the subchondral bone, including inhibited bone remodeling, slowed osteophyte development, and attenuated cancellous subchondral bone loss following loading, but had little effect on the progression of load-induced cartilage damage. We previously have observed a similar reduction in osteophyte maturity with ALN treatment concurrent with daily loading (*8*). In addition, multiple studies examining the role of bone remodeling in surgically induced posttraumatic OA models reported both a similar reduction of osteophyte development and attenuation of subchondral bone loss when bone remodeling is inhibited with bisphosphonate treatment (*17*, *49*). In contrast to our findings, ALN treatment immediately following a single bout of loading, which initiated OA, reduced cartilage degeneration (*18*, *50*). However, the lack of chondroprotection with ALN treatment in the present study is similar to previous results when ALN or another bisphosphonate treatment was concurrent with daily tibial loading (*8*), occurred during spontaneous OA development in guinea pigs (*51*), or administered to clinically diagnosed patients with OA (*52*). Together, these findings suggest that ALN may be chondroprotective when given immediately following a single initiating event that leads to subsequent posttraumatic OA development rather than in chronic or spontaneous OA phenotypes.

PTH pretreatment combined with ALN treatment concurrent with loading had an additive effect with protections against both load-induced cartilage degeneration provided by PTH pretreatment and subchondral bone changes provided by ALN treatment. To better understand the spatiotemporal progression of joint damage and the effects of PTH pretreatment and ALN treatment on OA progression, we examined transcriptomic changes across cartilage, bone, and lymph nodes at early time points after loading (Fig. 7). The combined PTH pretreatment and ALN treatment increased the number of DEGs in cartilage at 1 week relative to other treatment groups, indicating an early surge in biological activity (Fig. 7A). Increased expression of genes associated to cartilage homeostasis (*38*),

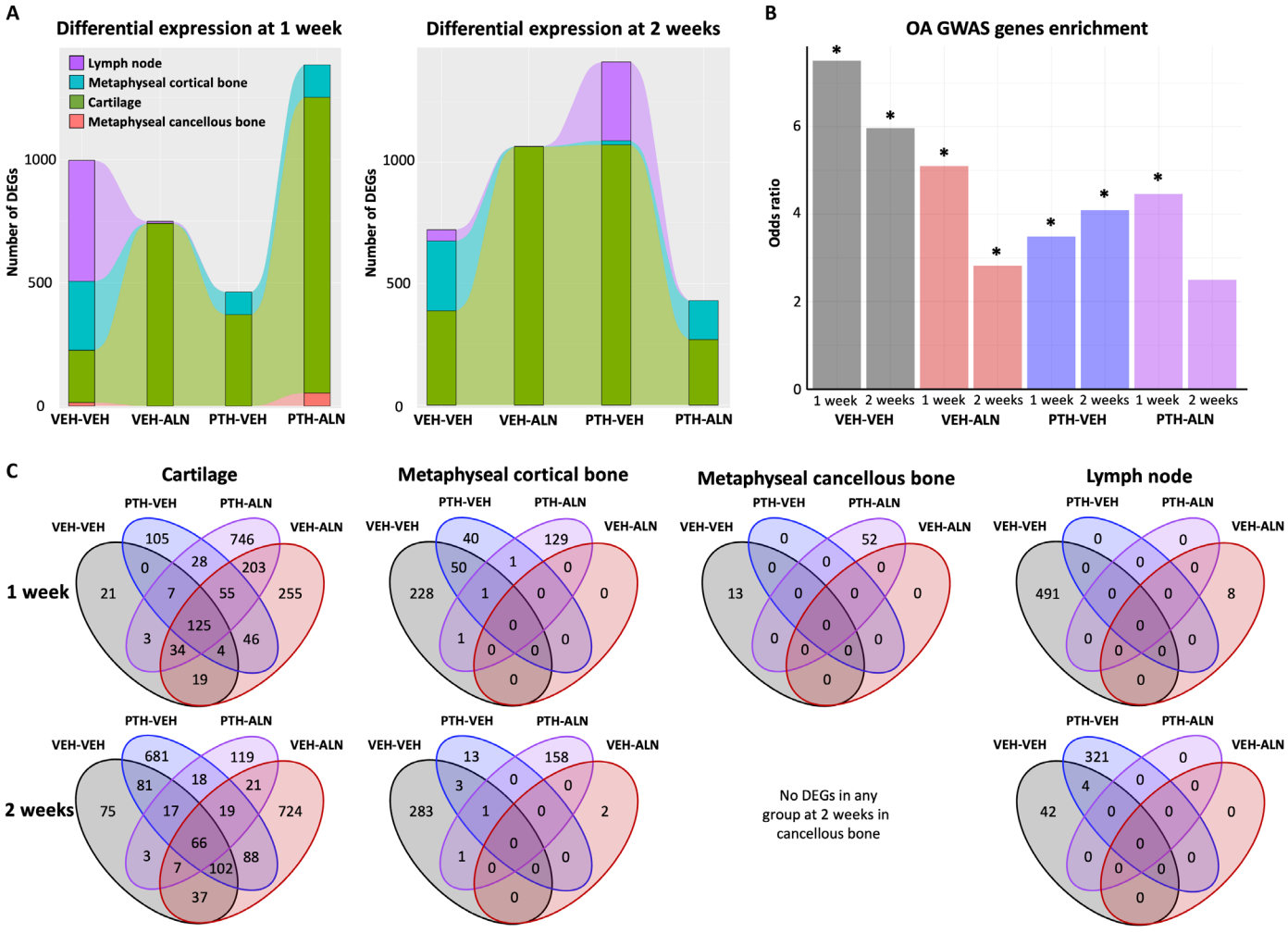

Fig. 7. Cross tissue visualization of loading, pretreatment, and treatment induced transcriptomic changes. (**A**) Alluvial diagrams of the DEGs between 1- and 2-week loaded limbs across tissues for each treatment group (FC > 2, FDR < 0.05). (**B**) Bar plot showing enrichment for OA-related genes calculated from GWAS in cartilage for each treatment group (odds ratio, FDR-corrected *P < 0.05 indicates significant enrichment). (**C**) Venn diagram representation of the DEGs between treatment groups for each tissue type following 1 or 2 weeks of loading (FC > 2, FDR < 0.05).

including *Acan*, *Sox9*, and *Col2a1*, suggest that the PTH-ALN co-treatment led to early reparative responses in cartilage that correlated to decreased tissue damage at later time points. In contrast, in the VEH-VEH group, increased cartilage structural damage and osteophyte formation observed at 6 weeks of loading corresponded with an early (1 week) increase in the expression of pathways involved in matrix remodeling and ossification in cartilage. Differential gene expression also was compared to OA-related genes from genome-wide associated studies (GWAS) (*53*). Genes identified by GWAS were no longer significantly enriched in the cartilage of the PTH-ALN group after 2 weeks of loading as compared to the VEH-VEH and other treatment groups (Fig. 7B).

Comparison of our differential gene expression and pathway analyses to recent single-cell RNA sequencing (scRNAseq) findings in cartilage (*54*–*57*) allowed us to draw further insight into differential expression associated with loading and treatment. In the PTH-ALN group, cartilage had up-regulation of pathways related to extracellular matrix organization and collagen fibril organization, both associated with changes in *Col2a1* and *Comp* gene expression. scRNAseq analysis of human OA cartilage defined a chondrocyte phenotype, reparative chondrocytes, identified by enrichment for both extracellular matrix signaling and collagen fibril organization pathways and expression of *Col2a1* and *Comp* (*56*). In contrast, up-regulation of matrix remodeling and ossification pathways both, associated with *Col10a1* and *Jun* expression, in the VEH-VEH group corresponded with gene expression profiles found in hypertrophic chondrocytes, which are known to contribute to catabolic metabolism and OA progression (*54*, *56*). Together, these findings suggest that PTH pretreatment combined with ALN treatment may influence chondrocyte phenotype, shifting gene expression profiles toward a reparative phenotype and away from a hypertrophic phenotype, thereby protecting cartilage from degeneration.

While immune responses and regulation of inflammation in OA primarily occur through the synovial tissue signaling (*58*), recent transcriptomic-based studies have identified alterations in genes and signaling pathways related to immune signaling in chondrocytes (*54*–*57*, *59*). Pathways containing genes linked to T cell receptor signaling and antigen presentation were down-regulated in cartilage at

1 week following loading in the PTH-ALN and PTH pretreatment-only groups. Similarly, PTH pretreatment before loading also downregulated expression of pathways containing genes linked to immune cell regulation. Chondrocytes have immunomodulatory capacities in vitro and are capable of suppressing activation, proliferation, and effector function of $CD4^+$ and $CD8^+$ T cells in coculture (*60*). Both $CD4^+$ and $CD8^+$ T cells are present in the synovium during OA progression and, through secretion of proinflammatory cytokines, contribute to cartilage degeneration and subchondral bone changes (*61*, *62*). However, the implications of suppressed T cell receptor signaling and antigen presentation for chondrocytes embedded in the extracellular matrix, where immune cell infiltration is limited, requires additional investigation. In scRNAseq, a chondrocyte phenotype, regulatory chondrocytes, was associated with early-stage OA progression and characterized by the expression of pathways related to T cell and B cell receptor signaling and antigen presentation (*54*). Regulatory chondrocytes play a regulatory role in OA progression and, given high expression of immune-specific markers found in this chondrocyte phenotype, are even speculated to have immune-related capacities within the cartilage extracellular matrix (*54*, *57*). Suppression of the characteristic regulatory chondrocyte pathways with PTH-ALN treatment may suggest that modulation of regulatory chondrocyte signaling attenuates OA progression (*57*). Overall, PTH pretreatment suppressed gene expression related to immune signaling pathways in cartilage. Our interpretation of these findings in relation to PTH effects on immune regulation and joint inflammation with OA progression remains limited by our lack of synovial tissue analyses.

PTH pretreatment and ALN treatment also altered load-induced differential gene expression in the lymph nodes and metaphyseal bone, giving further insight into the impact of treatment across the whole joint. PTH-ALN treatment eliminated an early increase in differential gene expression observed in the lymph node with VEH-VEH treatment, suggesting an early modulation of load-driven immune responses (Fig. 7, A and C). The association between early-stage differential gene expression responses in the lymph node and increased OA development over time could be of interest from a diagnostic biomarker perspective and requires further investigation. ALN treatment also modulated the proportion of B cells and $CD8^+$ T cells inferred from gene expression profiles in the lymph node. The proportion of $CD8^+$ T cells in the lymph node increased at 1 week with ALN treatment. Bisphosphonates induce γδ T cells and their regulation of inflammatory cytokines (*63*, *64*) potentially altering the inflammatory environment within the joint. We were unable to examine the proportion of γδ T cells in the inguinal lymph node using CIBERSORT in the present study. Both PTH pretreatment and ALN treatment altered the transcriptomic response with loading in cortical and cancellous bone. However, for transcriptomic analyses, bone samples were collected from the metaphysis, not the subchondral bone plate directly beneath the cartilage, which limits our ability to draw direct conclusions about the subchondral bone response and cross-talk between bone and cartilage in OA progression.

Our study has strengths and limitations. OA is a multifactorial disease caused by changes occurring in multiple tissues simultaneously and interdependently. By examining both tissue-level and transcriptomic changes across multiple tissues, we correlated early-stage transcriptomic changes with subsequent tissue-level structural damage and joint degeneration. However, bulk RNA-seq limited our ability to directly attribute signaling responses to specific cell populations. Because we used contralateral limbs as our loading controls, we also cannot identify whether systemic transcriptomic changes occurred because of loading or OA development. In addition, because of the challenge of simultaneously dissecting cartilage and adjacent subchondral bone from the same joint, we examined transcriptomic changes in the metaphyseal cortical and cancellous bone located below the growth plate, away from the joint surface. At the metaphysis, the response to loading likely was more anabolic and less reflective of OA development compared to subchondral bone directly beneath cartilage. Specifically, epiphyseal cancellous bone mass decreased with load-induced OA development in groups without ALN treatment, which likely would be evident in the transcriptomic response. Our transcriptomic results indicated suppression of immune-related pathways in cartilage with PTH pretreatment. Most prior work examining the role of joint inflammation and immune modulation in OA has focused on the role synovial tissue and synovium-cartilage cross-talk (*56*, *65*). In the present study, we uniquely examined transcriptomic changes in the lymph node to gain insight into the immune response but were unable to collect the synovium for RNA-seq limiting our mechanistic conclusions regarding the role of inflammation and immune modulation in PTH pretreatment and ALN treatment attenuating OA progression. Last, performing transcriptomic and IHC analysis at all time points would have provided additional insights throughout the course of the disease. However, given the large size of our study, we chose to prioritize these measures at early time points to identify gene and protein expression alterations that predated late-stage structural damage.

In conclusion, our results indicated that therapies targeting the subchondral bone can attenuate the progression of load-induced OA pathology and that a shift in chondrocyte phenotype likely plays a mechanistic role in the efficacy of these therapies in joint tissues. In addition, early transcriptomic signatures of cartilage and lymph nodes can potentially serve as predictors of tissue-level changes and OA pathology at later time points, improving our understanding of the multiscale relationships driving load-induced OA. Together, our findings suggest the treatment potential of subchondral bone-modifying therapies to slow the progression of early OA and the diagnostic potential of early transcriptomic signatures to detect signs of OA before visible radiographic changes.

MATERIALS AND METHODS

Treatment conditions and cyclic mechanical loading

PTH [PTH (1–34), 40 μg/kg per day, subcutaneous (*66*)] or VEH (saline, same volume, subcutaneous) pretreatment was administered for 8 weeks (5 days/week) to 18-week-old male C57BL/6 J mice (202 animals in total). Following pretreatment, cyclic mechanical loading was applied to the left tibia at a peak load of 9 N for 0 (pretreatment only, no loading; Fig. 1A), 1, 2, or 6 weeks (Fig. 2A) (*8*, *29*, *30*). Concurrent with loading, pretreated mice received either ALN [73 μg/kg per day, intraperitoneal (*18*)] or VEH (saline, same volume, intraperitoneal) treatment (5 days/week; Fig. 2A). Mice were placed under general anesthesia during loading (2% isoflurane, 1.0 liter/min, Webster). Loading was applied to the left tibiae at 4 Hz for 1200 cycles (5 min) per day, 5 days/week (*8*, *29*, *30*). The right tibiae served as contralateral controls. Following completion of the loading periods, mice were euthanized.

In a subset of mice following 1, 2, and 6 weeks of loading, knee joints were harvested and fixed in 4% paraformaldehyde (PFA) overnight at 4°C for tissue-level analysis ($n = 7$ to 8 per group). In the pretreatment-only group, right limbs were harvested and fixed in 4% PFA overnight at 4°C, and left limbs were frozen in phosphate-buffered saline (PBS)–soaked gauze immediately following dissection for nanoindentation analysis. In a separate group of mice following 0, 1, or 2 weeks of loading, different tissues (cartilage, inguinal lymph nodes, and metaphyseal cancellous and cortical bone, after bone marrow removal) were retrieved. Cartilage samples were stabilized in RNAlater, while inguinal lymph node and bone samples were snap frozen in liquid nitrogen for for RNA isolation and bulk RNA-seq analyses ($n = 4$ to 8 per group). RNA was extracted from tibial cartilage, metaphyseal cortical bone, cancellous bone, and inguinal lymph node tissues using protocols previously described (*67*, *68*) ($n = 4$ to 8/ea). Samples were not pooled. All experimental procedures were approved by the Institutional Animal Care and Use Committee at Cornell University and by the United States Army Medical Research and Development Command (USAMRMC) Animal Care and Use Review Office and are reported following ARRIVE guidelines (*69*) and best practices to implement and report experiments using the tibial loading model (*70*).

Nanoindentation of cartilage

Nanoindentation was used to assess the effects of PTH pretreatment on cartilage mechanical properties. Left limbs of PTH or VEH pretreatment-only groups ($n = 3$ per group) were defrosted, and the femur, ligaments, tendons, and the meniscus were dissected to expose the tibial cartilage. Tibial plateaus with exposed cartilage were glued to the surface of a microscope slide (Loctite 409, Henkel Corp., Rocky Hill, CT). During indentation, tibial cartilage was maintained in PBS to prevent dehydration. Nanoindentation was performed on the medial and lateral tibial condyles with a spherical tip (borosilicate particle, radius = 5 μm, Au coating, purchased from Novascan Technologies) using an atomic force microscope (Asylum-MF3D-Bio-AFM-SPM), as previously described (*71*). Indentation was repeated at seven to nine different locations per tibia.

Microcomputed tomography

MicroCT scans were used to assess subchondral bone morphological differences with PTH pretreatment and ALN treatment and in response to cyclic loading (Fig. 1A). After fixation in PFA, tissues were washed and transferred to 70% ethanol. Intact knee joints were scanned with an isotropic voxel resolution of 10 μm (μCT35, Scanco, Bruttisellen, Switzerland; 55 kVp, 145 μA, 600-ms integration time). Thickness and TMD of the subchondral cortical plate were measured at the proximal tibia. Bone volume fraction (BV/TV) and TMD were assessed in the tibial epiphysis. In all regions, bone was isolated by manually contouring the desired volume of interest (VOI). The VOI for the subchondral bone plate included the region of cortical bone beginning at the proximal end of the tibia and extended distally to the start of the cancellous bone in the epiphysis. The VOI of the epiphysis included cancellous bone distal to the subchondral plate and proximal to the growth plate.

Histological analysis

Following microCT scanning, knee joints were decalcified in 10% EDTA for 2 weeks, dehydrated in an ethanol gradient, and embedded in paraffin for histological analysis. Coronal sections of 6-μm thickness were obtained from posterior to anterior using a microtome (Leica RM2255, Wetzlar, Germany). Cartilage damage was assessed with Safranin O/Fast Green staining of the medial and lateral tibial plateaus at 90-μm intervals throughout the joint using OARSI histological scoring performed by a blinded researcher (*72*). OARSI scores are reported as a whole joint mean. Cartilage thickness was measured on three representative Safranin O/Fast Green stained sections (posterior, middle, and anterior) on both medial and lateral tibial plateaus as previously described (*8*, *18*, *29*, *30*). Cartilage thickness is reported as a whole-joint mean and a posterior-region mean.

Osteophyte formation in the medial tibia was assessed from Safranin-O/Fast Green–stained sections in loaded joints. Osteophyte size was defined as the medial-lateral width of the osteophyte at its widest point, measured from the medial edge of the epiphysis to the edge of the ectopic bone. Osteophyte maturity was scored on a scale of 0 to 3 (0 = no osteophyte, 1 = primarily cartilaginous, 2 = mixture of cartilage, and bone, or 3 = primarily bony structure) as previously described (*43*).

Immunohistochemistry

To investigate the impact of PTH pretreatment, ALN treatment, and mechanical loading in cartilage integrity, MMP-13, RUNX2, PTH1R, and sclerostin levels were measured in tibial cartilage by IHC analyses. All cartilage IHC was completed in the pretreatment-only and 1-week loaded groups (1 slide per limb, $n = 4$ mice per group). Sections were deparaffinized, rehydrated, and incubated in citric acid buffer for antigen retrieval at 60°C for 1 hour. Sections were incubated with 3% H_2O_2 solution for 10 min to quench endogenous peroxidase activity and then blocked with protein block from rabbit-specific horseradish peroxidase/3,3′-diaminobenzidine (HRP/DAB) (ABC) detection kit (ab64261, Abcam, Cambridge, UK) for 5 min. Sections were incubated overnight at 4°C overnight with anti-rabbit MMP-13 (1:50, ab39012), RUNX2 (1:50, ab23981), PTH1R (1:100, ab180762), or sclerostin (1:50, ab63097) polyclonal antibodies (Abcam, Cambridge, UK) or incubated with recombinant rabbit immunoglobulin (IgG) (1:50, ab172730) for negative controls. Sections were then treated with biotinylated goat anti-rabbit IgG(H + L) followed by streptavidin peroxidase for 10 min each [rabbit-specific HRP/DAB (ABC) detection kit, ab64261, Abcam, Cambridge, UK]. Last, sections were incubated with DAB chromogen solution [50X DAB chromogen with DAB substrate at 1:50 dilution, rabbit-specific HRP/DAB (ABC) detection kit, ab64261, Abcam, Cambridge, UK] for 5 min. Counterstaining was performed using hematoxylin for 1 min. Positive cells were stained brown. The total area of positive immunostaining in the articular cartilage of the medial and lateral tibial plateaus was calculated and normalized to cartilage area (ImageJ software, NIH), as described (*73*).

Bone remodeling and Wnt signaling were assessed in the epiphysis and metaphysis by IHC analysis in the pretreatment-only and 1-week loaded groups. Sections were stained for TRAP or procollagen I as previously described (*74*). The number of positively stained osteoclasts (TRAP) and osteoblasts (procollagen I) were quantified and normalized to measured bone surface (OsteomeasureXP v3.2.1.7). Osteoclast number was quantified for two slides per limb ($n = 7$ to 8 per group), and osteoblast number was quantified for one slide per limb ($n = 4$ per group). Sections were stained for sclerostin in bone following the same protocol as described above for cartilage. The number of sclerostin positive osteocytes were quantified and

normalized to the total number of osteocytes (1 slide per limb, $n = 4$ per group).

RNA sequencing

All methods were performed with sterile reagents under sterile conditions. Tissues were dissected as previously described (*24*, *31*, *67*). Briefly, tibial cartilage was microdissected from the proximal subchondral plate and isolated under a dissecting microscope while submerged in RNAlater. Cartilage samples were stored in RNAlater, and metaphyseal cancellous and cortical bone (Fig. 1A) and inguinal lymph node samples were flash frozen in liquid nitrogen. Trizol (Life Technologies, Carlsbad, CA) was added, and samples were pulverized (Tissue Lyser II, Qiagen, Germantown, MD, USA) for 6 min at 30 Hz in tubes containing 2.8-mm ceramic beads. RNA was isolated using a phenol-chloroform extraction (Qiagen RNeasy kit, Qiagen, Germantown, MD, with deoxyribonuclease digest) (*67*). All samples had an RNA quality number ≥ 6.0 (3730xl DNA Analyzer, Applied Biosystems, Waltham, MA, USA). 3′ RNA-seq was performed at the Cornell Genomics Core (NextSeq 500, Illumina, San Diego, CA) (*75*), which produces a single sequence per transcript to limit expression bias from longer transcripts.

Transcripts were aligned to the *mm10* genome [STAR (*76*)]. Each sample contained over 1 million of uniquely mapped reads to the mouse genome. Genes with less than three counts per million were not included for analysis. Differential expression between loaded and control limbs was determined using a paired design [edgeR (*77*)] and defined as genes with a fold change >2 or <−2 with a < 0.05 FDR. To examine biological processes, the $\log_2$fold change ranked gene list from the differential gene expression analysis was used to compute biological processes enriched with loading (clusterProfiler, Gene Ontology geneset, p.adj <0.05).

Selected tissue-specific genes with well described roles in the homeostasis and OA-related pathology were examined. To examine these individual genes, the normalized gene counts [reads per million mapped reads calculated in DESeq2 with Trimmed Mean of M-values correction (*78*)] were standardized between loaded and control limbs for each group.

CIBERSORT for immune cell analysis

CIBERSORT, a deconvolution-based algorithm that uses standardized gene expression data to calculate cell fractions based on gene expression profiles (*44*), was used to estimate proportion of immune cells in the inguinal lymph node at 0, 1, and 2 weeks. The gene composition of each cell was determined by calculating the expression level of each gene in each immune cell, with a mouse-specific gene archive containing eight types of immune cells (*79*). Normalized gene counts were used as inputs.

Statistical analysis

Histological scores, cartilage thickness, IHC measures, and bone parameters of PTH and VEH pretreatment-only (nonloaded) limbs were compared using a Student's *t* test. Cartilage stiffness of PTH and VEH pretreatment-only limbs were compared using a linear mixed-effects model with a fixed effect of pretreatment and a random mouse effect to account for repeated measurements with the same mouse limbs. The effects of loading, duration, pretreatment, and treatment were determined using a linear mixed-effects model with fixed effects of loading (contralateral control versus loaded), duration (1 week versus 2 weeks versus 6 weeks), pretreatment (PTH versus VEH) and treatment (ALN versus VEH), and a random mouse effect. Post hoc analysis was performed using Tukey's test for significant interaction effects and *t* test for individual effects. Normality was confirmed visually using histograms and QQ plots of the residuals. Significance was set at $P < 0.05$.

Supplementary Materials

This PDF file includes:

Figs. S1 to S9

Legends for data files S1 to S4

Other Supplementary Material for this manuscript includes the following:

Data files S1 to S4

REFERENCES AND NOTES

1. Y. Hu, X. Chen, S. Wang, Y. Jing, J. Su, Subchondral bone microenvironment in osteoarthritis and pain. *Bone Res.* **9**, 20 (2021).
2. M. B. Goldring, S. R. Goldring, Articular cartilage and subchondral bone in the pathogenesis of osteoarthritis. *Ann. N. Y. Acad. Sci.* **1192**, 230–237 (2010).
3. S. R. Goldring, M. B. Goldring, Changes in the osteochondral unit during osteoarthritis: Structure, function and cartilage-bone crosstalk. *Nat. Rev. Rheumatol.* **12**, 632–644 (2016).
4. E. L. Radin, R. M. Rose, Role of subchondral bone in the initiation and progression of cartilage damage. *Clin. Orthop. Relat. Res.* , 34–40 (1986).
5. J. Dequeker, J. Aerssens, F. P. Luyten, Osteoarthritis and osteoporosis: Clinical and research evidence of inverse relationship. *Aging Clin. Exp. Res.* **15**, 426–439 (2003).
6. A. Hartley, S. A. Hardcastle, L. Paternoster, E. McCloskey, K. E. S. Poole, M. K. Javaid, M. Aye, K. Moss, R. Granell, J. Gregory, M. Williams, J. H. Tobias, C. L. Gregson, Individuals with high bone mass have increased progression of radiographic and clinical features of knee osteoarthritis. *Osteoarthr. Cartil.* **28**, 1180–1190 (2020).
7. L. Chu, X. Liu, Z. He, X. Han, M. Yan, X. Qu, X. Li, Z. Yu, Articular cartilage degradation and aberrant subchondral bone remodeling in patients with osteoarthritis and osteoporosis. *J. Bone Miner. Res.* **35**, 505–515 (2020).
8. O. O. Adebayo, F. C. Ko, P. T. Wan, S. R. Goldring, M. B. Goldring, T. M. Wright, M. C. H. van der Meulen, Role of subchondral bone properties and changes in development of load-induced osteoarthritis in mice. *Osteoarthr. Cartil.* **25**, 2108–2118 (2017).
9. S. N. Ziemian, O. O. Ayobami, A. M. Rooney, N. H. Kelly, D. T. Holyoak, F. P. Ross, M. C. H. van der Meulen, Low bone mass resulting from impaired estrogen signaling in bone increases severity of load-induced osteoarthritis in female mice. *Bone* **152**, 116071 (2021).
10. M. Bellido, L. Lugo, J. A. Roman-Blas, S. Castaneda, J. R. Caeiro, S. Dapia, E. Calvo, R. Largo, G. Herrero-Beaumont, Subchondral bone microstructural damage by increased remodelling aggravates experimental osteoarthritis preceded by osteoporosis. *Arthritis Res. Ther.* **12**, R152 (2010).
11. M. Bellido, L. Lugo, J. A. Roman-Blas, S. Castaneda, E. Calvo, R. Largo, G. Herrero-Beaumont, Improving subchondral bone integrity reduces progression of cartilage damage in experimental osteoarthritis preceded by osteoporosis. *Osteoarthr. Cartil.* **19**, 1228–1236 (2011).
12. X. L. Yuan, H. Y. Meng, Y. C. Wang, J. Peng, Q. Y. Guo, A. Y. Wang, S. B. Lu, Bone-cartilage interface crosstalk in osteoarthritis: Potential pathways and future therapeutic strategies. *Osteoarthr. Cartil.* **22**, 1077–1089 (2014).
13. D. B. Burr, M. A. Gallant, Bone remodelling in osteoarthritis. *Nat. Rev. Rheumatol.* **8**, 665–673 (2012).
14. T. Hayami, M. Pickarski, Y. Zhuo, G. A. Wesolowski, G. A. Rodan, L. T. Duong, Characterization of articular cartilage and subchondral bone changes in the rat anterior cruciate ligament transection and meniscectomized models of osteoarthritis. *Bone* **38**, 234–243 (2006).
15. S. M. Botter, G. J. V. M. van Osch, J. H. Waarsing, J. C. van der Linden, J. A. N. Verhaar, H. A. P. Pols, J. P. T. M. van Leeuwen, H. Weinans, Cartilage damage pattern in relation to subchondral plate thickness in a collagenase-induced model of osteoarthritis. *Osteoarthritis Cartilage* **16**, 506–514 (2008).
16. S. Zhu, K. Chen, Y. Lan, N. Zhang, R. Jiang, J. Hu, Alendronate protects against articular cartilage erosion by inhibiting subchondral bone loss in ovariectomized rats. *Bone* **53**, 340–349 (2013).
17. T. Hayami, M. Pickarski, G. A. Wesolowski, J. McLane, A. Bone, J. Destefano, G. A. Rodan, L. T. Duong, The role of subchondral bone remodeling in osteoarthritis: Reduction of cartilage degeneration and prevention of osteophyte formation by alendronate in the rat anterior cruciate ligament transection model. *Arthritis Rheum.* **50**, 1193–1206 (2004).

18. S. N. Ziemian, A. M. Witkowski, T. M. Wright, M. Otero, M. C. H. van der Meulen, Early inhibition of subchondral bone remodeling slows load-induced posttraumatic osteoarthritis development in mice. *J. Bone Miner. Res.* **36**, 2027–2038 (2021).
19. J. C. Chang, A. Sebastian, D. K. Murugesh, S. Hatsell, A. N. Economides, B. A. Christiansen, G. G. Loots, Global molecular changes in a tibial compression induced ACL rupture model of post-traumatic osteoarthritis. *J. Orthop. Res.* **35**, 474–485 (2017).
20. A. Sebastian, D. K. Murugesh, M. E. Mendez, N. R. Hum, N. D. Rios-Arce, J. L. McCool, B. A. Christiansen, G. G. Loots, Global gene expression analysis identifies age-related differences in knee joint transcriptome during the development of post-traumatic osteoarthritis in mice. *Int. J. Mol. Sci.* **21**, 364 (2020).
21. K. M. Fisch, R. Gamini, O. Alvarez-Garcia, R. Akagi, M. Saito, Y. Muramatsu, T. Sasho, J. A. Koziol, A. I. Su, M. K. Lotz, Identification of transcription factors responsible for dysregulated networks in human osteoarthritis cartilage by global gene expression analysis. *Osteoarthr. Cartil.* **26**, 1531–1538 (2018).
22. J. Soul, S. L. Dunn, S. Anand, F. Serracino-Inglott, J. M. Schwartz, R. P. Boot-Handford, T. E. Hardingham, Stratification of knee osteoarthritis: Two major patient subgroups identified by genome-wide expression analysis of articular cartilage. *Ann. Rheum. Dis.* **77**, 423 (2018).
23. J. Steinberg, L. Southam, A. Fontalis, M. J. Clark, R. L. Jayasuriya, D. Swift, K. M. Shah, R. A. Brooks, A. W. McCaskie, J. M. Wilkinson, E. Zeggini, Linking chondrocyte and synovial transcriptional profile to clinical phenotype in osteoarthritis. *Ann. Rheum. Dis.* **80**, 1070–1074 (2021).
24. P. Singh, M. Wang, P. Mukherjee, S. G. Lessard, T. Pannellini, C. B. Carballo, S. A. Rodeo, M. B. Goldring, M. Otero, Transcriptomic and epigenomic analyses uncovered Lrrc15 as a contributing factor to cartilage damage in osteoarthritis. *Sci. Rep.* **11**, 21107 (2021).
25. D. W. Dempster, F. Cosman, M. Parisien, V. Shen, R. Lindsay, Anabolic actions of parathyroid hormone on bone. *Endocr. Rev.* **14**, 690–709 (1993).
26. D. B. Burr, T. Hirano, C. H. Turner, C. Hotchkiss, R. Brommage, J. M. Hock, Intermittently administered human parathyroid hormone(1-34) treatment increases intracortical bone turnover and porosity without reducing bone strength in the humerus of ovariectomized cynomolgus monkeys. *J. Bone Miner. Res.* **16**, 157–165 (2001).
27. R. G. G. Russell, N. B. Watts, F. H. Ebetino, M. J. Rogers, Mechanisms of action of bisphosphonates: Similarities and differences and their potential influence on clinical efficacy. *Osteoporos. Int.* **19**, 733–759 (2008).
28. J. C. Burket, D. J. Brooks, J. M. MacLeay, S. P. Baker, A. L. Boskey, M. C. H. van der Meulen, Variations in nanomechanical properties and tissue composition within trabeculae from an ovine model of osteoporosis and treatment. *Bone* **52**, 326–336 (2013).
29. F. C. Ko, C. Dragomir, D. A. Plumb, S. R. Goldring, T. M. Wright, M. B. Goldring, M. C. H. van der Meulen, In vivo cyclic compression causes cartilage degeneration and subchondral bone changes in mouse tibiae. *Arthritis Rheum.* **65**, 1569–1578 (2013).
30. D. T. Holyoak, M. Otero, N. S. Armar, S. N. Ziemian, A. Otto, D. Cullinane, T. M. Wright, S. R. Goldring, M. B. Goldring, M. C. H. van der Meulen, Collagen XI mutation lowers susceptibility to load-induced cartilage damage in mice. *J. Orthop. Res.* **36**, 711–720 (2018).
31. T. A. Wheeler, A. Y. Antoinette, E. Bhatia, M. J. Kim, C. N. Ijomanta, A. Zhao, M. C. H. van der Meulen, A. Singh, Mechanical loading of joint modulates t cells in lymph nodes to regulate osteoarthritis. *Osteoarthritis Cartilage* **32**, 287–298 (2024).
32. Q. Hu, M. Ecker, Overview of MMP-13 as a promising target for the treatment of osteoarthritis. *Int. J. Mol. Sci.* **22**, 1742 (2021).
33. T. Komori, H. Yagi, S. Nomura, A. Yamaguchi, K. Sasaki, K. Deguchi, Y. Shimizu, R. T. Bronson, Y. H. Gao, M. Inada, M. Sato, R. Okamoto, Y. Kitamura, S. Yoshiki, T. Kishimoto, Targeted disruption of results in a complete lack of bone formation owing to maturational arrest of osteoblasts. *Cell* **89**, 755–764 (1997).
34. P. Wang, M. Tortorella, K. England, A. M. Malfait, G. Thomas, E. C. Arner, D. Pei, Proprotein convertase furin interacts with and cleaves pro-ADAMTS4 (Aggrecanase-1) in the trans-Golgi network. *J. Biol. Chem.* **279**, 15434–15440 (2004).
35. K. Nagata, H. Hojo, S. H. Chang, H. Okada, F. Yano, R. Chijimatsu, Y. Omata, D. Mori, Y. Makii, M. Kawata, T. Kaneko, Y. Iwanaga, H. Nakamoto, Y. Maenohara, N. Tachibana, H. Ishikura, J. Higuchi, Y. Taniguchi, S. Ohba, U. I. Chung, S. Tanaka, T. Saito, *Runx2* and Runx3 differentially regulate articular chondrocytes during surgically induced osteoarthritis development. *Nat. Commun.* **13**, 6187 (2022).
36. C. Becher, T. Szuwart, P. Ronstedt, S. Ostermeier, A. Skwara, S. Fuchs-Winkelmann, C. O. Tibesku, Decrease in the expression of the type 1 PTH/PTHrP receptor (PTH1R) on chondrocytes in animals with osteoarthritis. *J. Orthop. Surg. Res.* **5**, 28 (2010).
37. W. Bouaziz, T. Funck-Brentano, H. Lin, C. Marty, H. K. Ea, E. Hay, M. Cohen-Solal, Loss of sclerostin promotes osteoarthritis in mice via β-catenin-dependent and -independent Wnt pathways. *Arthritis Res. Ther.* **17**, 24 (2015).
38. M. B. Goldring, M. Otero, Inflammation in osteoarthritis. *Curr. Opin. Rheumatol.* **23**, 471–478 (2011).
39. N. Fukui, Y. Ikeda, T. Ohnuki, N. Tanaka, A. Hikita, H. Mitomi, T. Mori, T. Juji, Y. Katsuragawa, S. Yamamoto, M. Sawabe, S. Yamane, R. Suzuki, L. J. Sandell, T. Ochi, Regional differences in chondrocyte metabolism in osteoarthritis: A detailed analysis by laser capture microdissection. *Arthritis Rheum.* **58**, 154–163 (2008).
40. P. Singh, K. B. Marcu, M. B. Goldring, M. Otero, Phenotypic instability of chondrocytes in osteoarthritis: On a path to hypertrophy. *Ann. N. Y. Acad. Sci.* **1442**, 17–34 (2019).
41. F. Tesche, N. Miosge, New aspects of the pathogenesis of osteoarthritis: The role of fibroblast-like chondrocytes in late stages of the disease. *Histol. Histopathol.* **20**, 329–337 (2005).
42. P. M. van der Kraan, W. B. van den Berg, Osteophytes: Relevance and biology. *Osteoarthr. Cartil.* **15**, 237–244 (2007).
43. C. B. Little, A. Barai, D. Burkhardt, S. M. Smith, A. J. Fosang, Z. Werb, M. Shah, E. W. Thompson, Matrix metalloproteinase 13-deficient mice are resistant to osteoarthritic cartilage erosion but not chondrocyte hypertrophy or osteophyte development. *Arthritis Rheum.* **60**, 3723–3733 (2009).
44. A. M. Newman, C. L. Liu, M. R. Green, A. J. Gentles, W. Feng, Y. Xu, C. D. Hoang, M. Diehn, A. A. Alizadeh, Robust enumeration of cell subsets from tissue expression profiles. *Nat. Methods* **12**, 453–457 (2015).
45. L. Liao, S. Zhang, J. Gu, T. Takarada, Y. Yoneda, J. Huang, L. Zhao, C.-D. Oh, J. Li, B. Wang, M. Wang, D. Chen, Deletion of *Runx2* in articular chondrocytes decelerates the progression of dmm-induced osteoarthritis in adult mice. *Sci. Rep.* **7**, 2371 (2017).
46. P. Orth, M. Cucchiarini, D. Zurakowski, M. D. Menger, D. M. Kohn, H. Madry, Parathyroid hormone [1-34] improves articular cartilage surface architecture and integration and subchondral bone reconstitution in osteochondral defects in vivo. *Osteoarthr. Cartil.* **21**, 614–624 (2013).
47. L. T. Shao, Y. Gou, J. K. Fang, Y. P. Hu, Q. Q. Lian, Y. Y. Zhang, Y. D. Wang, F. M. Tian, L. Zhang, Parathyroid hormone (1-34) ameliorates cartilage degeneration and subchondral bone deterioration in collagenase-induced osteoarthritis model in mice. *Bone Joint Res.* **9**, 675–688 (2020).
48. T. Bellido, A. A. Ali, I. Gubrij, L. I. Plotkin, Q. Fu, C. A. O'Brien, S. C. Manolagas, R. L. Jilka, Chronic elevation of parathyroid hormone in mice reduces expression of sclerostin by osteocytes: A novel mechanism for hormonal control of osteoblastogenesis. *Endocrinology* **146**, 4577–4583 (2005).
49. L. Zhang, H. Hu, F. Tian, H. Song, Y. Zhang, Enhancement of subchondral bone quality by alendronate administration for the reduction of cartilage degeneration in the early phase of experimental osteoarthritis. *Clin. Exp. Med.* **11**, 235–243 (2011).
50. M. S. Khorasani, S. Diko, A. W. Hsia, M. J. Anderson, D. C. Genetos, D. R. Haudenschild, B. A. Christiansen, Effect of alendronate on post-traumatic osteoarthritis induced by anterior cruciate ligament rupture in mice. *Arthritis Res. Ther.* **17**, 30 (2015).
51. M. Ding, C. C. Danielsen, I. Hvid, The effects of bone remodeling inhibition by alendronate on three-dimensional microarchitecture of subchondral bone tissues in guinea pig primary osteoarthrosis. *Calcif. Tissue Int.* **82**, 77–86 (2008).
52. C. O. Bingham III, J. C. Buckland-Wright, P. Garnero, S. B. Cohen, M. Dougados, S. Adami, D. J. Clauw, T. D. Spector, J.-P. Pelletier, J.-P. Raynauld, V. Strand, L. S. Simon, J. M. Meyer, G. A. Cline, J. F. Beary, Risedronate decreases biochemical markers of cartilage degradation but does not decrease symptoms or slow radiographic progression in patients with medial compartment osteoarthritis of the knee: Results of the two-year multinational knee osteoarthritis structural arthritis study. *Arthritis Rheum.* **54**, 3494–3507 (2006).
53. J. B. J. van Meurs, Osteoarthritis year in review 2016: Genetics, genomics and epigenetics. *Osteoarthr. Cartil.* **25**, 181–189 (2017).
54. Q. Ji, Y. Zheng, G. Zhang, Y. Hu, X. Fan, Y. Hou, L. Wen, L. Li, Y. Xu, Y. Wang, F. Tang, Single-cell RNA-seq analysis reveals the progression of human osteoarthritis. *Ann. Rheum. Dis.* **78**, 100–110 (2019).
55. A. Sebastian, J. L. McCool, N. R. Hum, D. K. Murugesh, S. P. Wilson, B. A. Christiansen, G. G. Loots, Single-cell RNA-seq reveals transcriptomic heterogeneity and post-traumatic osteoarthritis-associated early molecular changes in mouse articular chondrocytes. *Cells* **10**, 1462 (2021).
56. C. H. Chou, V. Jain, J. Gibson, D. E. Attarian, C. A. Haraden, C. B. Yohn, R. M. Laberge, S. Gregory, V. B. Kraus, Synovial cell cross-talk with cartilage plays a major role in the pathogenesis of osteoarthritis. *Sci. Rep.* **10**, 10868 (2020).
57. X. Kang, K. Zhang, Y. Wang, Y. Zhao, Y. Lu, Single-cell RNA sequencing analysis of human chondrocytes reveals cell-cell communication alterations mediated by interactive signaling pathways in osteoarthritis. *Front. Cell Dev. Biol.* **11**, 1099287 (2023).
58. S. R. Goldring, Alterations in periarticular bone and cross talk between subchondral bone and articular cartilage in osteoarthritis. *Ther. Adv. Musculoskelet. Dis.* **4**, 249–258 (2012).
59. E. A. Lewallen, C. A. Bonin, X. Li, J. Smith, M. Karperien, A. N. Larson, D. G. Lewallen, S. M. Cool, J. J. Westendorf, A. J. Krych, A. A. Leontovich, H. J. Im, A. J. van Wijnen, The synovial microenvironment of osteoarthritic joints alters RNA-seq expression profiles of human primary articular chondrocytes. *Gene* **591**, 456–464 (2016).
60. P. Lohan, O. Treacy, K. Lynch, F. Barry, M. Murphy, M. D. Griffin, T. Ritter, A. E. Ryan, Culture expanded primary chondrocytes have potent immunomodulatory properties and do not induce an allogeneic immune response. *Osteoarthr. Cartil.* **24**, 521–533 (2016).

61. J. E. Woodell-May, S. D. Sommerfeld, Role of inflammation and the immune system in the progression of osteoarthritis. *J. Orthop. Res.* **38**, 253–257 (2020).
62. E. B. P. Lopes, A. Filiberti, S. A. Husain, M. B. Humphrey, Immune contributions to osteoarthritis. *Curr. Osteoporos. Rep.* **15**, 593–600 (2017).
63. R. Casetti, A. Martino, The plasticity of gamma delta T cells: Innate immunity, antigen presentation and new immunotherapy. *Cell. Mol. Immunol.* **5**, 161–170 (2008).
64. R. Takimoto, T. Suzawa, A. Yamada, K. Sasa, Y. Miyamoto, K. Yoshimura, Y. Sasama, M. Tanaka, M. Kinoshita, K. Ikezaki, M. Ichikawa, M. Yamamoto, T. Shirota, R. Kamijo, Zoledronate promotes inflammatory cytokine expression in human CD14-positive monocytes among peripheral mononuclear cells in the presence of γδ T cells. *Immunology* **162**, 306–313 (2021).
65. E. Sanchez-Lopez, R. Coras, A. Torres, N. E. Lane, M. Guma, Synovial inflammation in osteoarthritis progression. *Nat. Rev. Rheumatol.* **18**, 258–275 (2022).
66. X. Yang, B. F. Ricciardi, A. Dvorzhinskiy, C. Brial, Z. Lane, S. Bhimani, J. C. Burket, B. Hu, A. M. Sarkisian, F. P. Ross, M. C. H. van der Meulen, M. P. Bostrom, Intermittent parathyroid hormone enhances cancellous osseointegration of a novel murine tibial implant. *J. Bone Joint Surg. Am.* **97**, 1074–1083 (2015).
67. C. Chlebek, J. A. Moore, F. P. Ross, M. C. H. van der Meulen, Molecular identification of spatially distinct anabolic responses to mechanical loading in murine cortical bone. *J. Bone Miner. Res.* **37**, 2277–2287 (2022).
68. N. H. Kelly, J. C. Schimenti, F. P. Ross, M. C. H. van der Meulen, Transcriptional profiling of cortical versus cancellous bone from mechanically-loaded murine tibiae reveals differential gene expression. *Bone* **86**, 22–29 (2016).
69. N. Percie du Sert, V. Hurst, A. Ahluwalia, S. Alam, M. T. Avey, M. Baker, W. J. Browne, A. Clark, I. C. Cuthill, U. Dirnagl, M. Emerson, P. Garner, S. T. Holgate, D. W. Howells, N. A. Karp, S. E. Lazic, K. Lidster, C. J. MacCallum, M. Macleod, E. J. Pearl, O. H. Petersen, F. Rawle, P. Reynolds, K. Rooney, E. S. Sena, S. D. Silberberg, T. Steckler, H. Wurbel, The ARRIVE guidelines 2.0: Updated guidelines for reporting animal research. *PLoS Biol.* **18**, e3000410 (2020).
70. R. P. Main, S. J. Shefelbine, L. B. Meakin, M. J. Silva, M. C. H. van der Meulen, B. M. Willie, Murine axial compression tibial loading model to study bone mechanobiology: Implementing the model and reporting results. *J. Orthop. Res.* **38**, 233–252 (2020).
71. B. Doyran, W. Tong, Q. Li, H. Jia, X. Zhang, C. Chen, M. Enomoto-Iwamoto, X. L. Lu, L. Qin, L. Han, Nanoindentation modulus of murine cartilage: A sensitive indicator of the initiation and progression of post-traumatic osteoarthritis. *Osteoarthr. Cartil.* **25**, 108–117 (2017).
72. S. S. Glasson, M. G. Chambers, W. B. Van Den Berg, C. B. Little, The OARSI histopathology initiative - recommendations for histological assessments of osteoarthritis in the mouse. *Osteoarthritis Cartilage* **18** (Suppl. 3), S17–S23 (2010).
73. K. L. Culley, S. G. Lessard, J. D. Green, J. Quinn, J. Chang, T. Khilnani, E. B. Wondimu, C. L. Dragomir, K. B. Marcu, M. B. Goldring, M. Otero, Inducible knockout of CHUK/IKKα in adult chondrocytes reduces progression of cartilage degradation in a surgical model of osteoarthritis. *Sci. Rep.* **9**, 8905 (2019).
74. K. M. Melville, N. H. Kelly, S. A. Khan, J. C. Schimenti, F. P. Ross, R. P. Main, M. C. H. van der Meulen, Female mice lacking estrogen receptor-alpha in osteoblasts have compromised bone mass and strength. *J. Bone Miner. Res.* **29**, 370–379 (2014).
75. S. Tandonnet, T. T. Torres, Traditional versus 3' RNA-seq in a non-model species. *Genom. Data* **11**, 9–16 (2017).
76. A. Dobin, C. A. Davis, F. Schlesinger, J. Drenkow, C. Zaleski, S. Jha, P. Batut, M. Chaisson, T. R. Gingeras, STAR: Ultrafast universal RNA-seq aligner. *Bioinformatics* **29**, 15–21 (2013).
77. M. D. Robinson, D. J. McCarthy, G. K. Smyth, edgeR: A Bioconductor package for differential expression analysis of digital gene expression data. *Bioinformatics* **26**, 139–140 (2010).
78. M. I. Love, W. Huber, S. Anders, Moderated estimation of fold change and dispersion for RNA-seq data with DESeq2. *Genome Biol.* **15**, 550 (2014).
79. Z. Chen, A. Huang, J. Sun, T. Jiang, F. X.-F. Qin, A. Wu, Inference of immune cell composition on the expression profiles of mouse tissue. *Sci. Rep.* **7**, 40508 (2017).

Acknowledgments: We thank E. Briggs, A. Otto, T. Wheeler, L. Lukashova, the Cornell Statistical Consulting Unit, the Cornell CARE staff, and the Genomic Facility at the Cornell Institute of Biotechnology. **Funding:** This work was funded by DOD PRMRP (W81XWH-17-1-0540), NIH (T32-AR007281) (S.N.Z. and M.C.H.v.d.M.), and The Clark Foundation. **Author contributions:** Conceptualization: A.Y.A., S.N.Z., T.M.W., S.R.G., M.B.G., M.O., and M.C.H.v.d.M. Methodology: A.Y.A., S.N.Z., C.C., M.O., and M.C.H.v.d.M. Investigation: A.Y.A., S.N.Z., A.R.B., and E.B.H. Visualization: A.Y.A. and S.N.Z. Funding acquisition: M.C.H.v.d.M., and S.N.Z. Project administration: M.C.H.v.d.M. Supervision: T.M.W., S.R.G., M.B.G., M.O., and M.C.H.v.d.M. Writing—original draft: A.Y.A. and S.N.Z. Writing—review and editing: A.Y.A., S.N.Z., A.R.B., E.B.H., C.C., T.M.W., S.R.G., M.B.G., M.O., and M.C.H.v.d.M. **Competing interests:** M.C.H.v.d.M. has grants/grants pending from NIH, NSF, and DOD and is a past president of the Orthopaedic Research Society. All other authors declare no competing interests. **Data and materials availability:** All tissue-level data and R code for sequencing analysis associated with this study are in the paper or Supplementary Materials. Raw gene counts for RNA-seq analysis are available to download through www.ncbi.nlm.nih.gov/geo/query/acc.cgi?acc=GSE253303.

Submitted 13 September 2023
Accepted 18 March 2024
Published 19 April 2024
10.1126/sciadv.adk8402